



**From experimental variability to the sorption related
retention parameters necessary for performance
assessment models for nuclear waste disposal systems:
The example of Pb adsorption on clay minerals**

Esra Orucoglu, Christophe Tournassat, Jean-Charles Robinet, Benoît Made,
Mélanie Lundy

► **To cite this version:**

Esra Orucoglu, Christophe Tournassat, Jean-Charles Robinet, Benoît Made, Mélanie Lundy. From experimental variability to the sorption related retention parameters necessary for performance assessment models for nuclear waste disposal systems: The example of Pb adsorption on clay minerals. Applied Clay Science, 2018, 163, pp.20 - 32. 10.1016/j.clay.2018.07.003 . insu-01857042

HAL Id: insu-01857042

<https://insu.hal.science/insu-01857042>

Submitted on 30 Sep 2020

HAL is a multi-disciplinary open access archive for the deposit and dissemination of scientific research documents, whether they are published or not. The documents may come from teaching and research institutions in France or abroad, or from public or private research centers.

L'archive ouverte pluridisciplinaire **HAL**, est destinée au dépôt et à la diffusion de documents scientifiques de niveau recherche, publiés ou non, émanant des établissements d'enseignement et de recherche français ou étrangers, des laboratoires publics ou privés.

From experimental variability to the sorption related retention parameters necessary for performance assessment models for nuclear waste disposal systems: the example of Pb adsorption on clay minerals.

Orucoglu Esra^{1,2*}, Tournassat Christophe^{1,2,3*}, Robinet Jean-Charles⁴, Madé Benoît⁴, Lundy Mélanie⁴

¹ *Institut des Sciences de la Terre d'Orléans, UMR 7327 Université d'Orléans–CNRS/INSU–BRGM, 45071 Orléans, France*

² *BRGM, 3 avenue Claude Guillemin, 45060 Orléans, France*

³ *Earth and Environmental Sciences Area, Lawrence Berkeley National Laboratory, Berkeley, CA 94720, USA*

⁴ *Andra, 1 – 7 rue Jean Monnet, 92298 Châtenay-Malabry, France*

*Corresponding authors: esra.orucoglu@cnrs-orleans.fr, c.tournassat@brgm.fr

Abstract

Surface complexation models (SCMs) have been developed in the last decades to describe metal ion sorption to clay minerals and especially to montmorillonite. In principle, these models can provide relevant information about sorption of radionuclides to be used in performance assessment (PA) of radioactive waste disposal systems. However, these SCMs have been developed in parallel with the acquisition of distinct adsorption datasets, which are not always consistent with each other. The objective of this study was to compare new experimental adsorption results with literature data to understand these discrepancies and to propose a SCM approach that could be amenable to determine sorption related retention parameters necessary for PA calculations. This study focused on lead (Pb) adsorption on montmorillonite, illite and in a natural clay (Callovo Oxfordian) as case studies of a strongly sorbing radionuclide that undergoes a range of retention processes depending on the chemical conditions. The experiments showed that many experimental artifacts lead to misinterpretations of the processes underlying the measured retention values. These include Pb precipitation in the presence of carbonate in solution. The determination of SCM parameters to provide sorption related information for PA of clay minerals should rely on preliminary building of an adequate adsorption database, where adequate means that all experimental conditions are met to quantify surface complexation only.

1. Introduction

In recent years, the scientific community has seen a remarkable surge of interest in the properties and behavior of clays as they apply to a variety of natural and engineered settings. Clay materials are known as an important part of the multi-barrier system for nuclear waste storage around the world, and their performance must be demonstrated on the time scale of hundreds to millions of years (Altmann 2008, Busch et al. 2008, Chapman and Hooper 2012, Armitage et al. 2013, Neuzil 2013). In these applications, the low hydraulic conductivity of the clay mineral-rich geological formations or of the engineered clay barriers provides at least part of the basis for isolating radionuclide contaminants (RN). Clay minerals have high adsorption capacity for a large range of radionuclides (Bradbury and Baeyens 2005a). The strong adsorption and resulting retardation of many contaminants by clay minerals make them ideal for use in natural or engineered barrier systems, particularly where there is a desire to improve confidence in the safety case beyond the reliance on slower transport rates alone (Altmann et al. 2012, Gaboreau et al. 2012, Borisover and Davis 2015, Grangeon et al. 2015). Because contaminant mobility in clay materials is mainly driven by diffusion and adsorption processes, a typical (simplified) scheme for estimating radionuclide release relies on knowing three parameters. The first is the effective diffusion coefficient (D_e), which quantifies the transport of each radionuclide across the barriers. The second is the distribution ratio of the radionuclide between the solution and the solid phases/surface (R_D or K_D if the retention is reversible), which quantifies the accumulation on the solid and the retardation of the radionuclide as it migrates from the repository across the barriers. The third is the solubility, which controls the maximum concentration in solution of the radionuclide of interest according to the geochemical conditions. These parameters are site specific, so to determine them specific data acquisition programs are needed. However, there is a fundamental difference between solubility and K_D values. Solubility values are usually obtained from the interpretation of experimental data with thermodynamic laws, which can be considered to be always valid, so solubility values can be applied to site-specific conditions, if environmental conditions such as temperature, pressure, and pore water composition are known, and with the assumption of precipitation/dissolution at thermodynamic equilibrium. Conversely, K_D values are directly measured in the presence of experimental conditions that are supposed to be representative of the *in situ* environmental conditions. As a direct consequence, knowledge about K_D values cannot be easily transferred from one site condition to another. For decades, quasi-thermodynamic models have been developed to predict the adsorption properties of many natural materials including clay minerals, oxides and organic matter. These models, grouped here under the term surface complexation models (SCM), aim to predict adsorption processes in a wide range of environmental conditions (Sposito 1984, Davis and Kent 1990, Dzombak and Morel 1990, Hiemstra and Van Riemsdijk 1996, Davis et al. 1998). If complete enough, they can be transferred from one site condition to another, providing that the dominant mechanisms have been identified and adequately quantified. In principle, these models could be used in performance assessment (PA) with calculations carried out with reactive transport codes. In practice, this is seldom the case, but recently, a hybrid approach, named “Smart K_D ”, which takes advantage of SCM flexibility with regards to changes in environmental conditions together with simplified models more amenable to PA calculations,

has been advanced to include more flexibility, predictability and transferability in these PA calculations (Richter et al. 2009, Stockmann et al. 2012, Druteikien et al. 2017). Near-field conditions will change over time following local perturbations induced by the presence of the waste repository. As an example, heat release from a radioactive waste package will temporarily increase the temperature that will itself influence the adsorption properties of clay minerals because of at least two processes. First, the affinity of the clay surfaces for a given RN is dependent on temperature (Tertre et al., 2005). Second, a temperature change influences the geochemical characteristics of the porewater, especially the pH, changing the distribution of species (speciation) in solution for the elements of interest (Gailhanou et al. 2017). So estimating SCM parameters and their associated uncertainties in as wide a range of conditions as possible is a key aspect in developing these PA approaches.

SCM parameters must be calibrated with experimental data in well-defined and well-controlled conditions. This is necessary in order to extrapolate the results in a wide range of conditions and to apply them to natural materials using a component additivity (CA) approach (Davis et al. 2004, Chen et al. 2014a, 2014b). The choice of the SCM is also important. A range of SCM that is applied to clay minerals and especially to montmorillonite have been developed and described in the literature (Zachara and Smith 1994, Bradbury and Baeyens 1997, Ikhsan et al. 2005, Gu and Evans 2007, Marcussen et al. 2009, Tertre et al. 2009, Gu et al. 2010, Akafia et al. 2011). These SCMs were developed in parallel with the acquisition of distinct adsorption datasets, which are not always consistent with each other (Tournassat et al. 2013). Several sources of discrepancies explain these inconsistencies, including differences in the properties of the clay materials (for example, natural variability in chemistry and size distribution, and preparation prior to experiments including sedimentation techniques and chemical treatments to remove mineral and organic impurities), differences in experimental procedures (order of reagent addition), and experimental artifacts. So the objective of this study was to compare new experimental adsorption results with literature data in order to understand these discrepancies and to propose a SCM approach that could be amenable to the determine sorption related retention parameters necessary for PA calculations. This study was focused on Pb adsorption as a case study of a strongly sorbing radionuclide on montmorillonite, illite and a natural clay mineral (Callovian-Oxfordian) (COx) that undergoes a range of retention processes as a function of chemical conditions.

2. Material and Methods

2.1. Overview of Experiments

Batch adsorption experiments were conducted with three different reference clay minerals, namely two montmorillonites (MX-80 and Kunipia-P) and one illite, and with a natural clay mineral assemblage present in COx claystone, in order to quantify the main adsorption mechanisms of Pb on clays. To clarify the effect of each of these mechanisms, various adsorption experiments were designed spanning a range of different solid/liquid ratio (R_{SL} in $g \cdot L^{-1}$), ionic strength (NaCl as a background electrolyte), pH, temperature, and initial Pb concentrations (Table 1).

Table 1. Summary of experimental conditions used with three different reference clays (purified MX-80, Kunipia and illite and one clay fraction of COx claystone).

Initial Pb concentration (μM)	R_{SL} ($\text{g}\cdot\text{L}^{-1}$)	NaCl concentration (M)	pH range	T ($^{\circ}\text{C}$)
1	1	0.1	3-9	20*
10	1	0.1	3-9	20*
50	1	0.1	3-9	20*
1	0.5	0.025	3-9	20*
1	1	0.1	3-7	67

* Room temperature

2.2. Chemicals

All chemicals used in the experiments were analytical grade: $\text{Pb}(\text{NO}_3)_2$ (Prolab R.P. Normapur, > 99.5%), NaCl (Merck, 99.6%), 30% HCl (Merck, Suprapur), NaOH pellets (Merck, > 99%), 65% HNO_3 (VWR Prolabo, 69.4% for cleaning, and Merck, Suprapur for AAS measurements), acetic acid ($\text{C}_2\text{H}_4\text{O}_2$, VWR Prolab, 96%), citric acid ($\text{C}_6\text{H}_8\text{O}_7\cdot\text{H}_2\text{O}$, Carlo Erbar, >99.8%), sodium bicarbonate (NaHCO_3 , ACS Amresco), 30% H_2O_2 (Merck), sodium dithionite ($\text{Na}_2\text{S}_2\text{O}_4$), MES ($\text{C}_6\text{H}_{13}\text{NO}_4\text{S}$, Sigma Aldrich, >99%), MOPS ($\text{C}_7\text{H}_{15}\text{NO}_4\text{S}$, Sigma Aldrich, >99.5%), tri sodium citrate dehydrate ($\text{C}_6\text{H}_5\text{Na}_3\text{O}_7\cdot 2\text{H}_2\text{O}$, Fluka, 99.99%). Milli-Q 18 M Ω water was used in all solution preparation, clay suspension and clay purification processes.

2.3. Solution Preparation

NaCl stock solutions (0.1 M and 0.025 M) were prepared from crystalline NaCl. HCl stock solution (1 mM) and NaOH stock solution (1 mM) were prepared from 30% HCl acid solution and NaOH pellets, respectively. Two 1 mM Pb stock solutions at two different ionic strength were prepared by dissolving crystalline $\text{Pb}(\text{NO}_3)_2$ in a 1 mM HCl / 0.1 M NaCl solution and in a 1 mM HCl solution. For experiments conducted with low Pb concentrations, 10 and 100 μM stock solutions were prepared by diluting these solutions in a 1 mM HCl / 0.1 M NaCl solution and in a 1 mM HCl solution. All solutions were prepared in an air atmosphere.

2.4. Clay Material

Clay stock dispersions with a solid / liquid ratio of 2 $\text{g}\cdot\text{L}^{-1}$ were prepared in a 0.1 M NaCl solution background for two montmorillonites (MX-80, and Kunipia-P), one purified illite (Illite du Puy, IdP), and the clay fraction of COx claystone. MX-80 montmorillonite was extracted from a stock of MX-80 bentonite and the clay fraction of COx claystone was obtained from the core EST 51779 (borehole OHZ6126 – depth: -476.5 m), which was drilled from the main gallery of Andra's Underground Research Laboratory sited at Bure in the Meuse district (LSMHM, France). The borehole was extracted from a formation level that is representative of the clayey unit of the COx formation; COx argillite mineralogical composition is made of clay minerals (mainly illite, mixed layer illite/smectite, kaolinite, mica and chlorite), tectosilicates (mainly quartz and feldspars) as well as carbonates (mainly calcite and dolomite) (Gaucher et al. 2004).

The clay fraction of this COx claystone is named hereafter COx clay. MX-80 and COx clay were separated and purified in four stages with a procedure which was already published (Jackson 1975, Tournassat et al. 2007, 2011). A fine clay particle fraction ($<2\ \mu\text{m}$) was separated by sedimentation and/or centrifugation according to Stoke's law. Carbonates were removed by adding 0.1 M acetic acid in 0.5 M NaCl (pH ~ 5) and the clays were then washed with three cycles of centrifugation and re-dispersion in 0.5 M NaCl solution. The above treatment was repeated twice. Next Fe and Mn oxides were removed with DCB (dithionite–citrate–bicarbonate) treatment using dithionite diluted in 0.2 M citrate ($\text{C}_6\text{H}_8\text{O}_7 \cdot \text{H}_2\text{O}$), 0.5 M NaCl, 0.1 M NaHCO_3 . The clays were then washed with three cycles of centrifugation and re-dispersion in 0.5 M NaCl solution. The above treatment was repeated twice. Finally, organic matter was removed with 3% H_2O_2 , 0.5 M NaCl solution at 60°C . After cooling, the clays were washed with three cycles of centrifugation and re-dispersion in 0.5 M NaCl solution. Centrifugation steps were carried out in Sigma 6K 10 Bioblock Scientific centrifuge at 13000 g for 30 min at 20°C . The extracted clay fraction of MX-80 usually contains minor amounts ($< 20\%$) of quartz, cristobalite and amorphous silica impurities (Gailhanou et al. 2007, Tournassat et al. 2009). The COx clay composition was not determined in this study and was considered to be representative of the clay fraction of the claystone, i.e. approximately 50% illite and 50% illite smectite mixed layer minerals (IS). Purified Illite du Puy (IdP) was obtained from a previous project. Its preparation procedure and characterization is described elsewhere (Gaboreau et al. 2016). The purified material was composed of illite layers (90–94%) and negligible smectite layer (4–6%) and K-feldspar (less than 5%). Kunipia-P is a highly purified Na-montmorillonite that contains nearly 100% montmorillonite, and that is produced by Kunimine Industries Co. Ltd. (Tachi and Yotsuji 2014).

2.5. Adsorption Experiments

The following procedure was used for all experimental conditions summarized in Table 1. First, Thermo Scientific™ Nalgene™ Oak Ridge High-Speed Polypropylene centrifuge tubes were acid treated (HNO_3) and washed three times with Milli-Q water before use. Then, 5 or 10 mL of the clay stock dispersion was equilibrated at the target ionic strength and pH by adding the correct amount of Milli-Q water, 0.1 M or 0.025 M NaCl, 0.01 M or 0.1 M HCl and 0.01 M or 0.1 M NaOH stock solutions to reach a total volume of 18 or 19 mL. In order to minimize the uncertainty on R_{SL} , the stock solution was stirred with a magnetic stirrer during its sampling. Then, 1 or 2 mL of acidified Pb stock solution (10 μM , 100 μM or 1 mM) was added to reach the target total Pb concentration (1 μM , 10 μM or 50 μM). The final pH value was always lower than the initial pH after clay dispersion pre-equilibration because the Pb stock solutions were acid. This acid addition corresponded to approximately 20 μL 0.1 M HCl per tube. At near neutral pH value, the pH value dropped by 1 to 1.5 pH units. A preliminary kinetic experiment showed that steady-state Pb concentration was reached after a few hours in the conditions tested. As a result, a contact time of four days was chosen in order (i) to ensure steady state in the system, and (ii) to be in agreement with contact times of one to seven days considered in other similar studies reported in the literature (Gu and Evans 2007, Gu et al. 2010, Marques Fernandes et al. 2015). Samples at room temperature were put on a horizontal shaker (Heidolph Rotamax 120) during the equilibration time.

One of the objectives of this study was to understand the variation of clay mineral affinity for lead in response to a moderate increase of temperature expected in the environment of radioactive waste disposal. For this reason, experiments were conducted at 67°C. For these experiments, the pH was initially adjusted at room temperature with addition of NaOH and HCl solutions. Clay dispersions were then heated and equilibrated for seven days at 67°C. Pb was then added at 67°C and the clay dispersions were equilibrated for four days at 67°C in a DigiPREP dry bath heater and were frequently agitated manually to re-suspend the settled clay particles. Additionally control samples were prepared for each of the experiment conditions. They were prepared with the same procedure except that the clay stock dispersion was replaced by NaCl stock solutions. C_{init} was determined from their average Pb concentrations at pH values below 6.5.

All preparations were done in an air atmosphere except a few experiments that were carried out in a N₂ atmosphere glove-box (MBraun Unilab) with stock solutions that were prepared inside the glove-box with Milli-Q that was degassed with N₂-bubbling in order to purge their CO₂/bicarbonate/carbonate content. In the glove-box, seven sorption experiments were conducted with 50 µM Pb, MX-80 clay at 5.7-9.4 pH range. For these samples, an aliquot of the clay stock dispersion was degassed by letting it equilibrate with the glove-box atmosphere for ten days. In addition, three control experiments were prepared without clay at pH 6.3 and 9.6. They were prepared with the same procedure as described above except that the clay stock dispersion was replaced by 0.1 M NaCl solutions.

After equilibration, samples were centrifuged at ~12700 g for 15 minutes in Sigma 6K 10 Bioblock Scientific centrifuge. For the samples equilibrated at 67°C the centrifuge temperature was set at 40 °C (the maximum value), and the samples were then put back into the dry bath heater at 67°C for a few hours. pH was measured at 67°C after calibration of the electrode response at 67°C. Then a 5 mL aliquot of supernatant was acidified with ~20 µL of 65% M HNO₃ in polystyrene tubes for Pb measurements. Another 5 mL aliquot was preserved without acidification for measurements (especially alkalinity). The volume of HNO₃ solution added was taken into account for correcting the measurement of final Pb concentration. Additional control experiments without addition of Pb solution made it possible to measure the release of Pb into solution naturally present in the clay minerals.

In addition to the samples investigated with the above procedure, some tests were also run to study the effect of the order of reagent addition (pH set before or after Pb addition), as well as the presence of pH buffers (sodium acetate/acetic acid at pH 3.6-4.6, MES at pH 5.5-6, and MOPS at pH 6.5-7), i.e. buffers whose use has been frequently reported in adsorption experiments described in the literature (Baeyens and Bradbury 1997, Marques Fernandes et al. 2016)) and filtering (0.1 µM Millex Syringe filters) the supernatant before Pb measurement. All of these tests were carried out with Kunipia-P montmorillonite.

2.6. Concentration and pH Measurements

An InLab micro electrode (Mettler Toledo) was used to measure the final pH in the supernatant of centrifuged dispersions. Before use, the tubes dedicated to Pb measurements were washed with 5% HNO₃ acid and then rinsed repeatedly with Milli-Q water. Pb concentrations were measured by furnace atomic absorption spectroscopy (AAS 220 Z, Spectra AA) or by inductively coupled-plasma mass spectrometry for the lowest

concentrations (ICP-MS-NEXION 350 X, Perkin Elmer). The comparison of AAS and ICP-MS independent measurement results also made it possible to control the accuracy of the measurements. Alkalinity was measured with an automatic titrator (736 GP Titrino Metrohm), using the Gran method. Dissolved inorganic carbon (DIC) concentrations were calculated from alkalinity and pH values.

2.7. Quantification of Adsorption

Surface coverage (C_{ads} in $\text{mol}\cdot\text{kg}^{-1}$) and distribution coefficient (R_D in $\text{L}\cdot\text{kg}^{-1}$) were calculated from the initial Pb concentration (C_{init} in $\text{mol}\cdot\text{L}^{-1}$), the equilibrium Pb concentration in solution (C_{eq} in $\text{mol}\cdot\text{L}^{-1}$) and the solid/liquid ratio (R_{SL} in $\text{kg}\cdot\text{L}^{-1}$).

$$C_{ads} = \frac{C_{init} - C_{eq}}{R_{SL}} \quad (1)$$

$$R_D = \frac{C_{init} - C_{eq}}{C_{eq} \times R_{SL}} \quad (2)$$

The error bands were calculated as follows (Tournassat et al. 2013):

$$uC_{ads} = \frac{\sqrt{uC_{init}^2 + uC_{eq}^2}}{R_{SL}}; \Delta C_{ads} = k \times uC_{ads} \quad (3)$$

$$uR_D = \sqrt{\left(\frac{uC_{init}}{R_{SL} \cdot C_{eq}}\right)^2 + \left(\frac{C_{init} \cdot uC_{eq}}{R_{SL} \cdot C_{eq}^2}\right)^2}; \Delta R_D = k \times R_D \quad (4)$$

Where Δ values are the considered error bands, k is the coverage factor ($k=2$, corresponding to a 95% confidence interval), uC_{init} and uC_{eq} are the uncertainties associated with the total concentration and the equilibrium concentration respectively, considered at 2% of the values. Uncertainty of the R_{SL} was neglected.

2.8. Modeling

The modeling of the data combined ion exchange on basal sites, surface complexation on edge sites and precipitation reactions. Geochemical modeling was carried out with PHREEQC v3 (Parkhurst and Appelo 2013). The ThermoChimie v9b database (Giffaut et al. 2014) was used to calculate aqueous and precipitation/dissolution reactions. The influence of the complexation reactions in solution (e.g. Pb^{2+} with Cl^- and HCO_3^-) was thus explicitly taken into account. The Debye-Huckel equation was used for ionic strength correction. In ThermoChimie, the temperature dependence of the equilibrium constants is estimated with the Van't Hoff equation. A standard temperature of 25°C was considered to model the data obtained at 20°C. The software PHREEPLOT was used to plot predominance diagrams and contour plots (Kinniburgh and Cooper 2011).

Sorption model parameters for ion exchange and surface complexation reactions were determined by a fitting procedure applied to the whole dataset, starting from the determination of selectivity coefficients for cation exchange reactions using experimental data sets at two different ionic strength and at low pH values. Then the surface complexation constants and the surface site densities were determined with the data measured in the pH range from 4 to 6.5.

3. Results

3.1. Influence of Experimental Procedures on Pb Retention

3.1.1. pH Buffers and Filtration

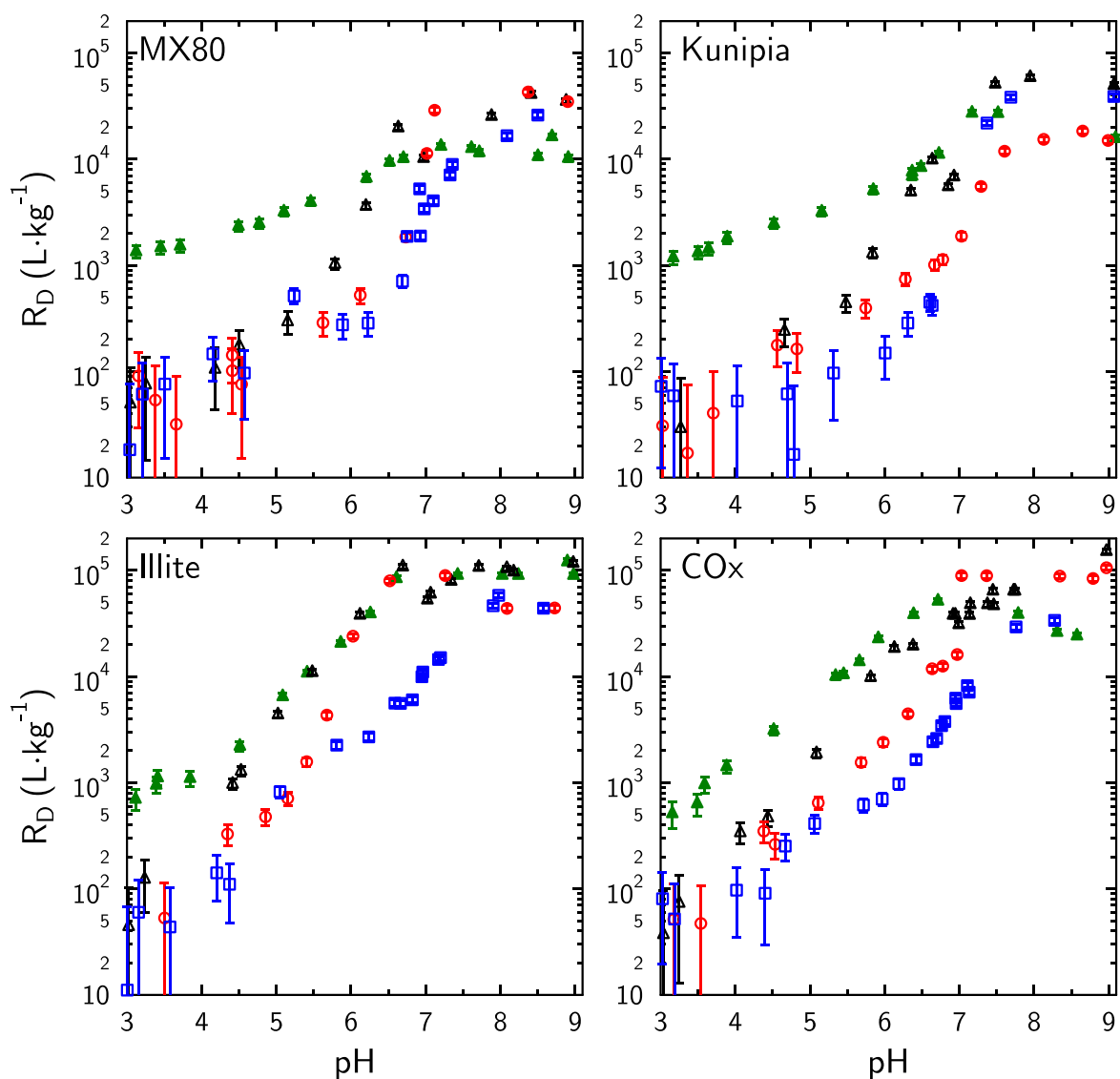
Adding buffers to stabilize the pH had a marked impact on the measured R_D and surface coverage (C_{ads}) values (Figure S-1, Supporting information), contrasting with the results of previous studies, which showed that the presence of pH-buffers had little or no effect on the adsorption of divalent metals on montmorillonite (Baeyens and Bradbury 1997). Because it was very difficult to fix the pH at a desired value without using a buffer, this experimental artefact prevented the acquisition of a Pb adsorption edge as a function of concentration and at constant pH. Instead, the Pb adsorption edge was established at constant Pb concentration and as a function of pH, with various total Pb concentrations from 1 μ M to 50 μ M. Using filters had little impact on the Pb concentration measurements at equilibrium. Consequently, Pb concentration was measured without filtering of the supernatant in agreement with procedures frequently reported in clay adsorption studies (Baeyens and Bradbury 1995, Yang et al. 2010, Marques Fernandes et al. 2015).

3.1.2. Order of Addition of Reagents

The order of addition of reagents had a big impact on the measured R_D values especially for pH values above 6, i.e. for pH values that necessitated the addition of NaOH to reach the target value: the addition of Pb prior to pH adjustment increased the measured retention of Pb compared to the case where Pb was added after pH adjustment. (Figure S-2). Consequently, the pH adjustments were done before spiking the solution with Pb in all experiments reported in the following.

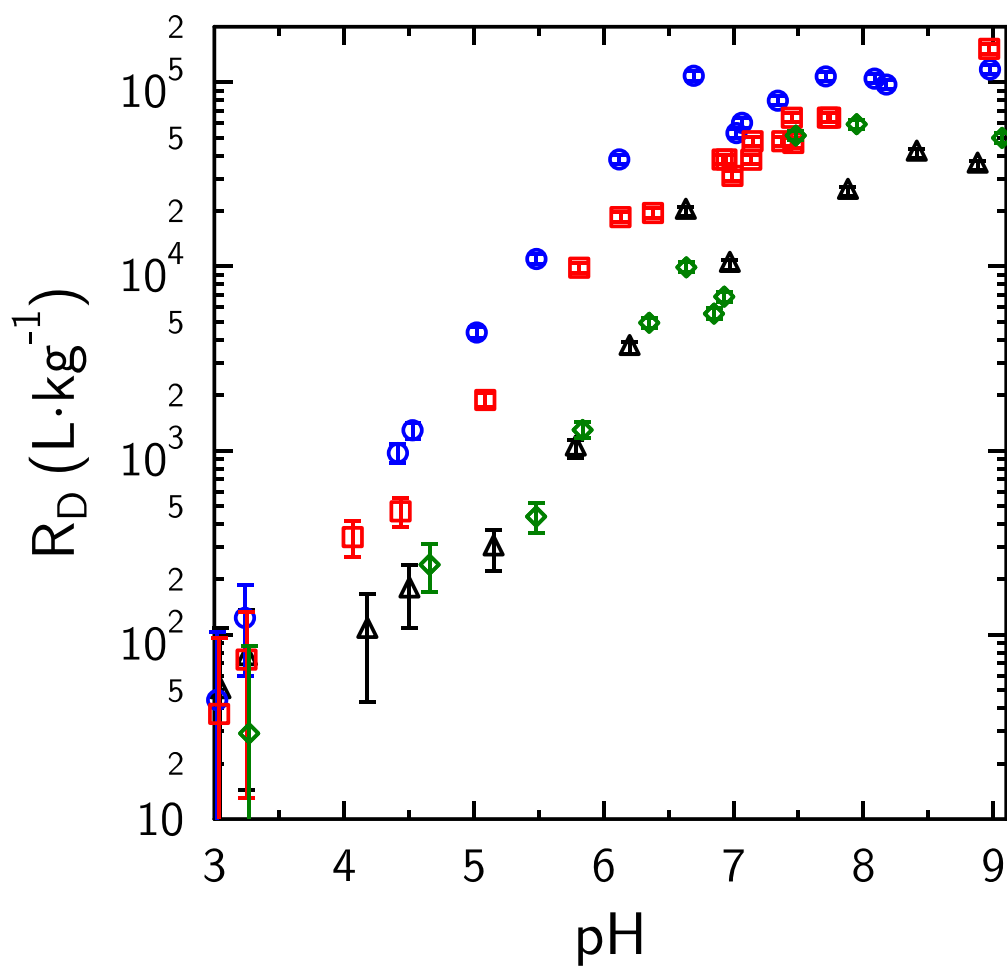
3.2. Pb Retention Behavior under Varying Chemical Conditions

Similar trends were observed for pH-dependent retention isotherms with all clay minerals at different ionic strengths (Figure 1) and at different total Pb concentrations. At room temperature, Pb retention increased with decreasing ionic strength at constant Pb concentration and constant pH, and it increased with increasing pH at constant ionic strength and total Pb concentration. Although similar in shape for all clay samples, Pb retention curves exhibited contrasted retention maxima depending on the clay samples' nature (Figure 2). Kunipia and MX-80 had very similar affinity for Pb and were the materials tested that had lowest Pb affinity. IdP had the greatest affinity, and COx clay sample exhibited retention behavior intermediate between montmorillonite and IdP, in qualitative agreement with its mineralogical composition containing illite and illite smectite mixed layers. The effect of ionic strength on retention was maximum at pH value below 5 for montmorillonite (MX-80 and Kunipia), and was otherwise limited. Changes in ionic strength had little effect on overall Pb retention for IdP and COx clay samples. A temperature increase had also no significant effect on Pb adsorption for all clay types in the investigated conditions ($C_{tot}=1 \mu$ M, 0.1 M NaCl, and 67°C) (Figure 3).



309

310 Figure 1. Comparisons of experimental datasets for Pb retention at room temperature on MX-
 311 80, Kunipia-P, IdP and COx clay as a function of pH, ionic strength (0.025 M NaCl = closed
 312 symbols; 0.1 M NaCl = open symbols), and total Pb initial concentrations (triangle symbols: 1
 313 μM ; circle symbols: 10 μM ; square symbols: 50 μM) (Details of the datasets are given in
 314 supporting information file).



315
 316 Figure 2. Comparison of Pb retention on MX-80 (triangles), Kunipia (diamonds), IdP (circles)
 317 and COx clay (squares) at room temperature as a function of pH, in the presence of 0.1 M
 318 NaCl background electrolyte and a total Pb concentration of 1 μ M.

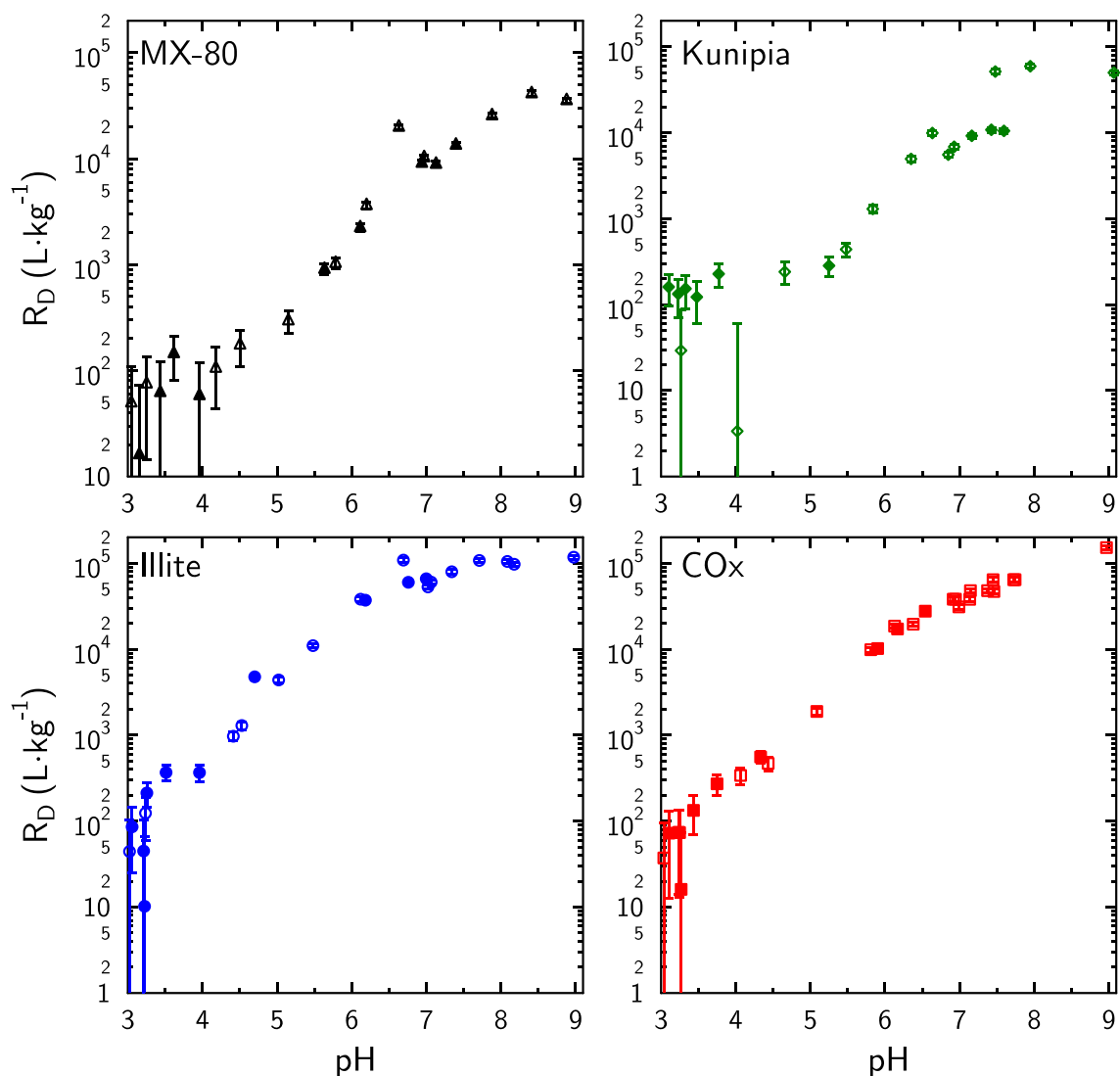


Figure 3. Pb retention on MX-80 (triangles), Kunipia (diamonds), IdP (circles) and COx clay (squares) at room temperature (open symbols) and 67°C (closed symbols) as a function of pH, in the presence of 0.1 M NaCl background electrolyte and a total Pb concentration of 1 μM (Details of the datasets are given in supporting information file).

3.3. Alkalinity and DIC concentrations

Samples tested at room temperature had alkalinity values within the range 0.17-0.31 $\text{meq}\cdot\text{L}^{-1}$ in the presence or absence of clay and for pH ranging from ~5.5 to 9. These alkalinity values corresponded to calculated DIC concentrations that were consistent with a near equilibrium of stock solutions and dispersion with atmospheric CO_2 ($\log p\text{CO}_2 = -3.5$) before the adsorption experiment (Figure 4, bottom) at pH 7-8. For this reason, a constant DIC concentration of ~0.25 $\text{mmol}\cdot\text{L}^{-1}$ (-3.6 in \log_{10} scale) was considered to be present in all samples. Despite the care to exclude CO_2 from the experiment conducted in the glove-box, alkalinity/DIC concentration values were similar to values obtained in experiments conducted outside the glove-box (Figure 4, bottom). This observation echoes the results of Tournassat et al. (2018) on U(VI) adsorption experiments on montmorillonite, where the DIC concentrations measured in “ CO_2 -free” experiment ranged from $8.2 \cdot 10^{-3}$ to $6.2 \cdot 10^{-2} \text{ mmol}\cdot\text{L}^{-1}$ in the pH range 3.9-9.9.

4. Modelling and Discussion

4.1. Adsorption versus (Co-)Precipitation

It is well known that divalent heavy metals such as Pb can precipitate at near natural or alkaline conditions depending on their concentration in the aqueous solution and on the water composition (Marani et al. 1995, Echeverría et al. 2005, Sipos et al. 2008, Tournassat et al. 2013). Thermodynamic calculations evinced that for a total Pb concentration of 50 μM , Pb precipitation was expected to occur at pH ~ 6.7 in the presence of atmospheric CO_2 partial pressure ($\log p\text{CO}_2 = -3.5$) (Figure 4, top). Therefore Pb precipitation could have occurred in the form of cerussite (PbCO_3), hydrocerussite ($\text{Pb}_3(\text{CO}_3)_2(\text{OH})_2$) or laurionite (PbClOH) above pH 6.7 for the highest investigated total Pb concentration (50 μM). Based on experiments with direct precipitation in solution, Marani et al. (1995) showed that cerussite and hydrocerussite can indeed form easily in conditions similar to the experimental conditions in this work. Pb (co-)precipitation may explain the discrepancy observed between experiments with Pb addition made before or after pH adjustment (Figure S-2): increasing the pH after Pb addition could have been responsible for (surface) precipitation when the concentrated NaOH solution entered into contact with the clay-Pb dispersion. Such (surface) precipitation and/or surface polymerization in the presence of clay minerals was evidenced in previous studies using EXAFS (Strawn and Sparks 1999) and by direct SEM observations (Echeverría et al. 2005), but with total Pb concentrations higher than those used in this study. In practice, data interpretation with an adsorption model needs to be restricted to the pH domain where precipitation does not occur (Tournassat et al. 2013). Consequently, the complexation of free Pb^{2+} by bicarbonate and carbonate in solution as well as the possible precipitation of Pb carbonate minerals must be taken into account for the quantitative interpretation of the results with SCM.

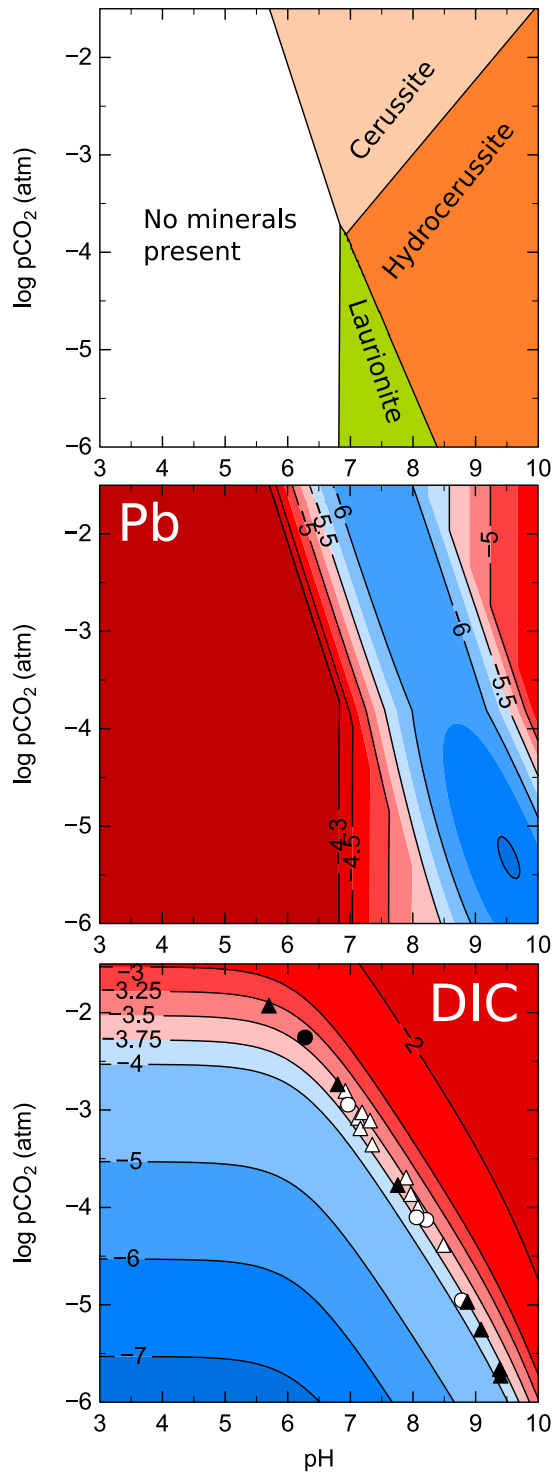


Figure 4. Top figure: Pb solid phase predominance as a function of pH and $p\text{CO}_2$ in the absence of adsorption processes. Minerals allowed to precipitate: cerussite (PbCO_3), hydrocerussite ($\text{Pb}_3(\text{CO}_3)_2(\text{OH})_2$), cotunnite (PbCl_2), laurionite (PbClOH), paralaurionite (PbClOH) and $\text{Pb}(\text{OH})_2(\text{s})$: Total Pb concentration: $50 \mu\text{M}$ ($\log [\text{Pb}]_{\text{tot}} = -4.3$). Middle figure: Contour plot of calculated Pb concentration in solution (\log_{10} scale) as a function of pH and $p\text{CO}_2$. The color change between two contour lines indicates a change of $0.25 \log_{10}$ scale units. Bottom figure: Contour plot of calculated DIC concentration as a function of pH and $p\text{CO}_2$ (\log_{10} scale). Symbols correspond to experimental measurements in the presence (triangles) or absence (circles) of clay and with sample preparation in contact with atmosphere

(white symbols) or in the glove-box (black symbols). The background electrolyte concentration is 0.1 M NaCl for all figures.

The data, obtained with correct reagent addition order, and in conditions where Pb precipitation was not expected from a thermodynamic point of view, were in qualitative agreement with the adsorption mechanisms of divalent metals on clay mineral surfaces that have been identified for many years, using a combination of wet chemistry experiments with diffractometric and spectrometric characterization (Tournassat et al. 2013, Borisover and Davis 2015). According to these mechanisms, cation exchange on basal and interlayer surfaces was responsible for Pb adsorption at low pH (below 3 to 5 depending on the clay material) where nearly constant R_D values were measured. As expected, changes in ionic strength impacted R_D values more for montmorillonite than for illite (Figure 2) because the cation exchange capacity of montmorillonite is higher than that of illite. R_D values with COx clay, which has intermediate cation exchange capacity between montmorillonite and illite, accordingly exhibited intermediate behavior. Surface complexation on the edge surfaces was responsible for Pb adsorption at higher pH, and a strong influence of pH on R_D values was recorded for all four types of samples. Note also that little effect of ionic strength was recorded.

4.2. Modeling Pb adsorption on clay mineral surfaces

4.2.1. Choice of model

SCMs quantify adsorption processes based on a set of protonation/deprotonation and adsorption reactions, which links the surface charge to the surface potential and the specific surface area where the reactions taken place. SCMs were initially developed to model the reactivity of oxide surfaces and gave rise to numerous variants, of which the most extensively used are the Constant Capacitance Model – CCM – (Goldberg 2013), Diffuse-Double Layer model – DDL – (Dzombak and Morel 1990), the Triple Layer Model – TLM – (Davis and Kent 1990), and the Charge Distribution model – CD(-MUSIC) – (Hiemstra and Van Riemsdijk 1996). Numerous SCM using these classical approaches have been published in the literature to describe adsorption on clay mineral surfaces (Zachara and Smith 1994, Turner et al. 1998, Barbier et al. 2000, Ikhsan et al. 2005, Gu and Evans 2007, Gu et al. 2010, Akafia et al. 2011). These models, however, have not taken into account the unique characteristics of electrostatic surface potentials that occur at clay edge sites, where the electrostatic surface potential of basal plane cation exchange sites influences the surface potential of neighboring edge sites, i.e. the ‘spillover’ effect (Secor and Radke 1985, Chang and Sposito 1996). Indeed, the spillover effect invalidates the use of classical SCMs such as DDL, CCM and TLM to quantify the effect of clay edge surface charge potential on adsorption (Bourg et al. 2007, Tournassat et al. 2013, 2016). The inadequacy of the classical DLM model to reproduce divalent metal adsorption on montmorillonite surface in a wide range of pH and ionic strength conditions has been put forward repeatedly for more than twenty years (Baeyens and Bradbury 1997, Akafia et al. 2011). Only recently, a SCM that included the spillover effect in the evaluation of the surface potential was successfully applied to quantify U(VI) adsorption on montmorillonite in a wide range of pH, ionic strength and DIC concentration conditions (Tournassat et al. 2018). In this study, quantifying Pb adsorption were investigated on montmorillonite samples, but also on illite samples and on a natural assemblage of illite,

illite/smectite mixed layer mineral (IS) and smectite. A second objective was the prediction of adsorption properties of natural Callovian-Oxfordian claystone in the presence of *in situ* conditions (pH~7.2 and $p\text{CO}_2 \sim 10^{-2}$ bar at 25°C). Unfortunately, the above mentioned ‘spillover’ model has been developed only for montmorillonite, not for illite. Alternatively, instead of a comprehensive model that includes as many physically grounded mechanisms as possible, simpler, yet successful, models can be developed. A good example of this kind of model is the 2SPNE SC/CE Model (2 site protolysis non-electrostatic surface complexation and cation exchange model) developed by Bradbury and Baeyens (1997). The authors noted that their data were better fitted if the electrostatic term was canceled. In this model, surface complexation of divalent metals on the clay mineral edge surfaces was ascribed to two types of sites: high-energy (strong) sites that are present in low amounts (typically $\sim 2 \text{ mmol}\cdot\text{kg}^{-1}$) and have high affinity for the adsorbate, and low energy (weak) sites that, conversely, are present in large amounts (typically $\sim 50 \text{ mmol}\cdot\text{kg}^{-1}$) and have low affinity for the adsorbate. Because this type of model aims for efficiency and simplicity and because it does not include physical features that play a significant role in the adsorption mechanism, it must fulfil the parsimony rule, i.e. that the least number of parameters must be considered to fit the data (Tournassat et al. 2013). In this modeling effort, this approach was applied together with a non-electrostatic model in order to fit the adsorption data on IdP and MX-80 samples, and then it was used to predict the adsorption on Kunipia and COx clay. The component additivity (CA) approach was used to model the adsorption on the COx clay with the assumption that the reactivity of edge site of illite/smectite mixed layers was similar to this combination of montmorillonite and illite layer edges (Davis et al. 2004, Chen et al. 2014a, 2014b).

4.2.2. Modeling the data at room temperature

A very simple model with only one cation exchange site and one edge surface complexation site (Table 2) was sufficient to fit all the data at room temperature (Figure 5 and Figure 6). The cation exchange selectivity coefficients for Pb on MX-80 and IdP ($\log K = 0.6$ and 0.7 respectively) had values similar to values reported for other divalent metals (e.g. Ni, Cu, Co, Zn, Fe) (Fletcher and Sposito 1989, Bradbury and Baeyens 2005a, Charlet and Tournassat 2005, Tournassat et al. 2009). The surface complexation site density values (0.01 and $0.035 \text{ mol}\cdot\text{kg}^{-1}$ for MX-80 and IdP respectively) were in the range of low energy site densities described in the literature for montmorillonite and illite, indicating that high energy sites may not be present on these samples or may be present at very low site density (Baeyens and Bradbury 1997, Bradbury and Baeyens 2005b). The presence of an additional high energy adsorption site in this model did not improve markedly the overall fitting of the data, so it was decided not to include it. The protonation of the surface was not needed in this model to fit the data (Tournassat et al. 2013). In the presence of high total Pb concentration and near neutral to alkaline pH values, (hydro)cerussite precipitation was in quantitative agreement with the observed sharp R_D increase. Retention data on Kunipia were adequately predicted with the same model as for MX-80. Retention data on COx clay were well predicted with a model mixing 50% of illite and 50% of montmorillonite. These proportions correspond roughly to the proportion of, respectively, illite and illite smectite mixed layers minerals in the clay fraction of the COx clay (Gaucher et al. 2004, Chen et al. 2014a) and indicate that the

456 reactivity of illite smectite mixed layers minerals can be modeled with edge surface
457 adsorption properties similar to those of montmorillonite.

458 Table 2. Parameters used in the non-electrostatic SCM at 25°C (values in parenthesis are for
459 67°C).

	Montmorillonite	Illite
Cation exchange		
CEC (X^- site density) in $\text{mol}\cdot\text{kg}^{-1}$	0.78 ⁽¹⁾	0.2 ⁽²⁾
Reactions	log K	
$2 X\text{Na} + \text{Pb}^{2+} = X_2\text{Pb} + 2 \text{Na}^+$	0.6 (0.9)	0.7 (0.9)
$2 X\text{Na} + \text{Mg}^{2+} = X_2\text{Mg} + 2 \text{Na}^+$	0.6	0.7
$2 X\text{Na} + \text{Ca}^{2+} = X_2\text{Ca} + 2 \text{Na}^+$	0.5	0.5
Edge surface complexation		
Site density ($>S$) in $\text{mol}\cdot\text{kg}^{-1}$	0.01	0.035
Reactions	log K	
$>\text{SOH} = >\text{SO}^- + \text{H}^+$	-8.1	-6.6
$>\text{SOH} + \text{Pb}^{2+} = >\text{SOPb}^+ + \text{H}^+$	0 (0.2)	0.6 (0.9)
$>\text{SOH} + \text{Pb}^{2+} + \text{H}_2\text{O} = >\text{SOPb}(\text{OH}) + 2\text{H}^+$	Not necessary	-7.2 (-6.7)

460 ⁽¹⁾(Bradbury and Baeyens 2002)

461 ⁽²⁾(Bradbury and Baeyens 2000)

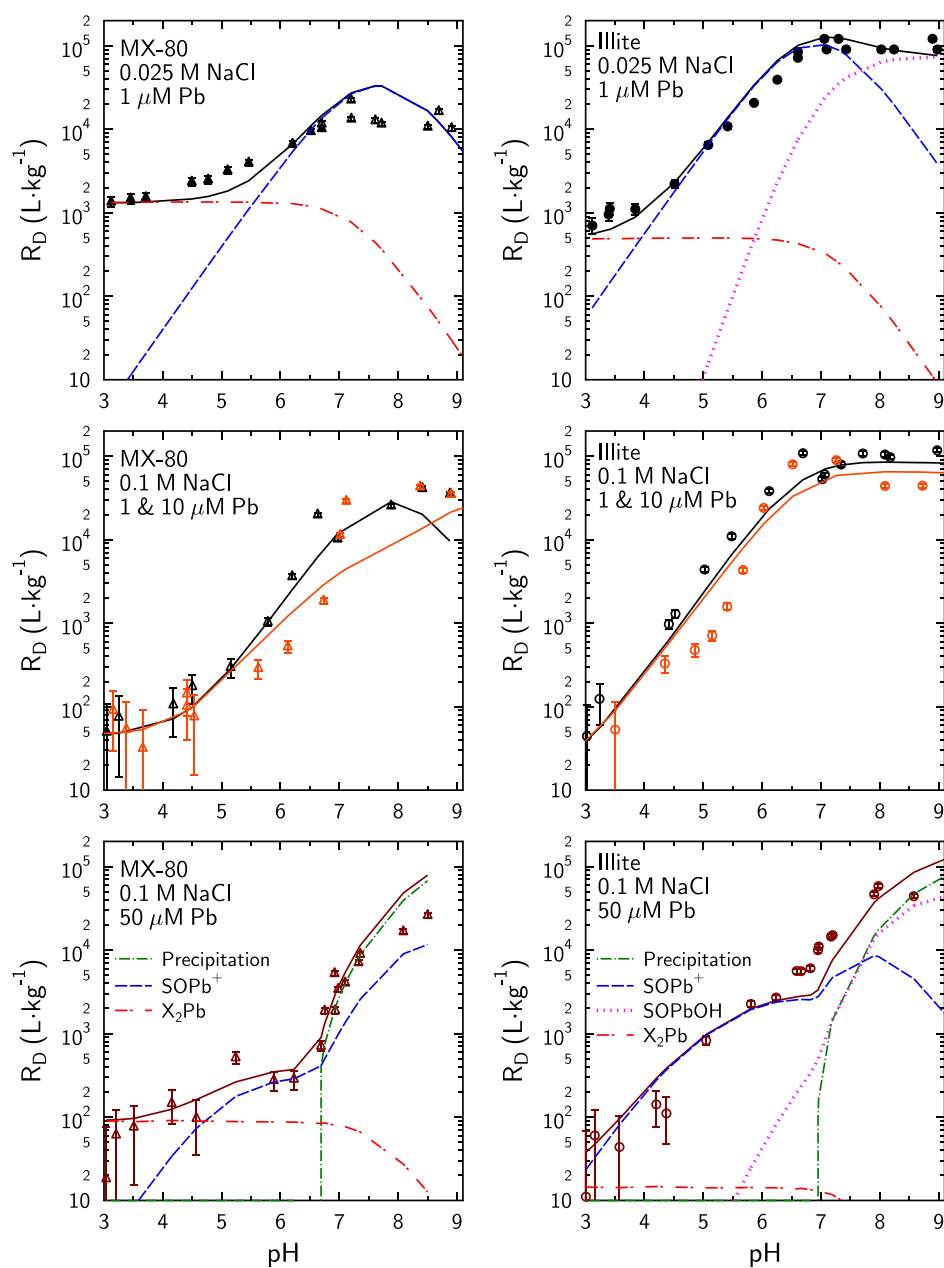


Figure 5. Modeling of Pb adsorption and precipitation at room temperature according to the parameters given in Table 2 for MX-80 (left) and illite (right).

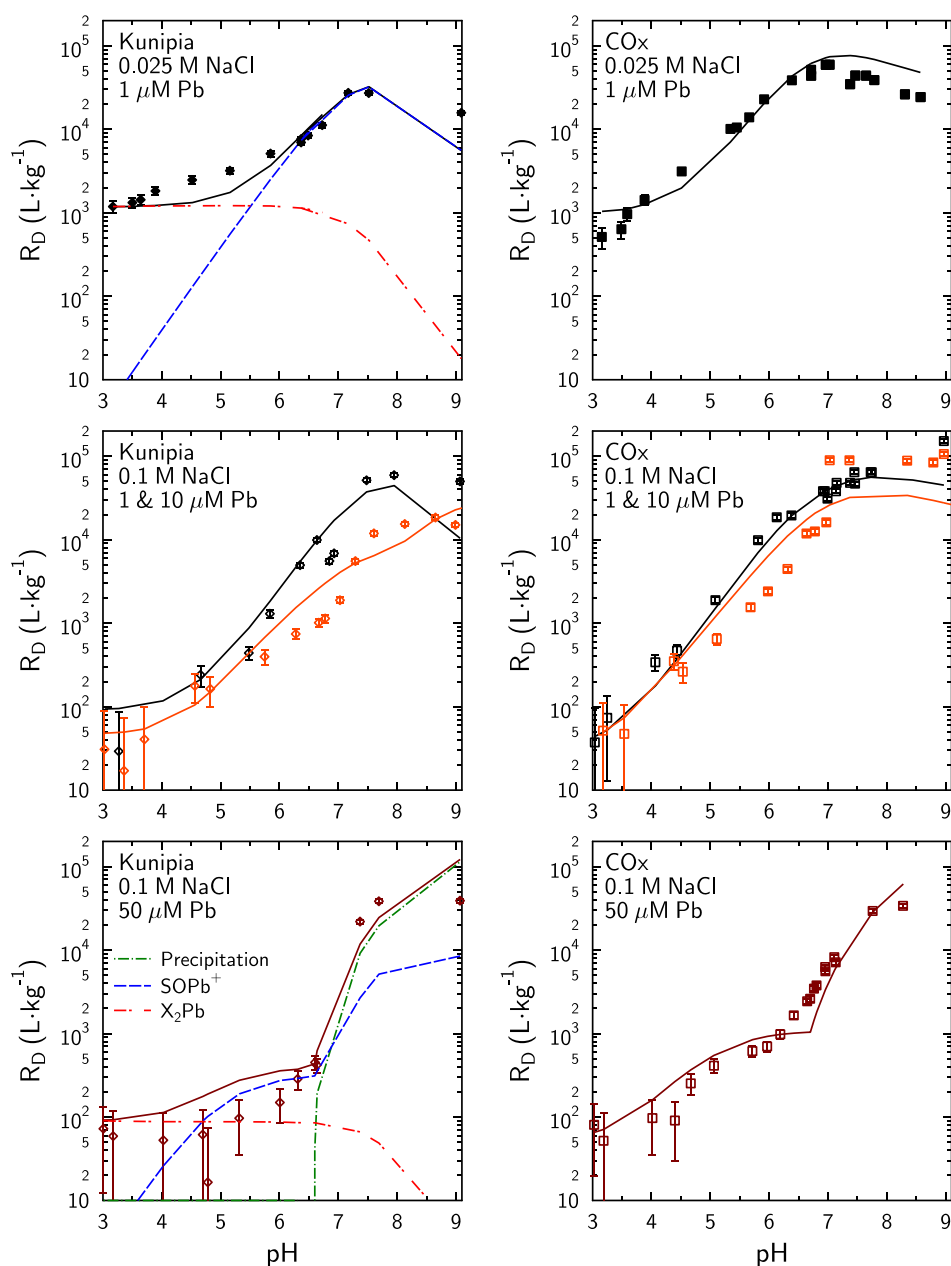


Figure 6. Model prediction for Pb adsorption / precipitation on Kunipia-P (left) and COx clay (right) at room temperature. Model parameters for Kunipia-P are the same as for MX-80. Pb adsorption on COx clay was modeled with an illite surface contribution of 50% and a smectite surface (montmorillonite) contribution of 50%.

4.2.3. Modeling the data at 67°C

A temperature increase at fixed pH and total Pb concentration values is responsible for a change in the $(\text{Pb}^{2+})/(\text{H}^+)$ activity ratio, which reflects the changes in Pb speciation in solution and the change of water dissociation constant as a function of temperature. This change should impact the equilibrium of the reaction $>\text{SOH} + \text{Pb}^{2+} = >\text{SOPb}^+ + \text{H}^+$. $(\text{Pb}^{2+})/(\text{H}^+)$ changes can be tracked by looking at the value of $(\text{Pb}^{2+})/(\text{H}^+)$ at 67°C normalized to its value at 25°C at fixed pH and total Pb concentration (Figure S-3). Up to pH 6, the value of

477 $\frac{(\text{Pb}^{2+})/(\text{H}^+)_{67^\circ\text{C}}}{(\text{Pb}^{2+})/(\text{H}^+)_{25^\circ\text{C}}}$ is nearly constant and close to 0.85. For pH values above 6, the value of
 478 $\frac{(\text{Pb}^{2+})/(\text{H}^+)_{67^\circ\text{C}}}{(\text{Pb}^{2+})/(\text{H}^+)_{25^\circ\text{C}}}$ decreases mostly because the abundance of Pb^{2+} compared to other Pb species
 479 in solution decreases with increasing pH faster at 67°C than at 25°C. A temperature increase
 480 from room temperature to 67°C had no significant effect on Pb adsorption on all four clay
 481 samples up to pH 7 (Figure 3). Therefore, a slight log K change was applied in this surface
 482 complexation model to compensate for the change in $(\text{Pb}^{2+})/(\text{H}^+)$ activity ratio in solution
 483 from room temperature to 67°C (Table 2, Figure 7). The log K of surface complexation
 484 reactions increased slightly with a temperature increase in agreement with previous
 485 observations made on Ni adsorption (Tertre et al. 2005). It could be tempting to conclude that
 486 a temperature increase is favorable to Pb adsorption on clay minerals. However, in a claystone
 487 such as the Callovo-Oxfordian clay the pH value is expected to decrease from ~7.2 at 20-
 488 25°C to ~6 at 80°C and the DIC concentration is expected to increase from ~3 mM at 20-
 489 25°C to ~15 mM at 80°C (Beaucaire et al. 2012, Gailhanou et al. 2017). Overall, these
 490 changes should be detrimental to Pb adsorption on clay mineral surfaces. Based on these
 491 results, it can be estimated that Pb adsorption R_D value should drop by approximately one
 492 order of magnitude if Pb is present at trace concentrations.

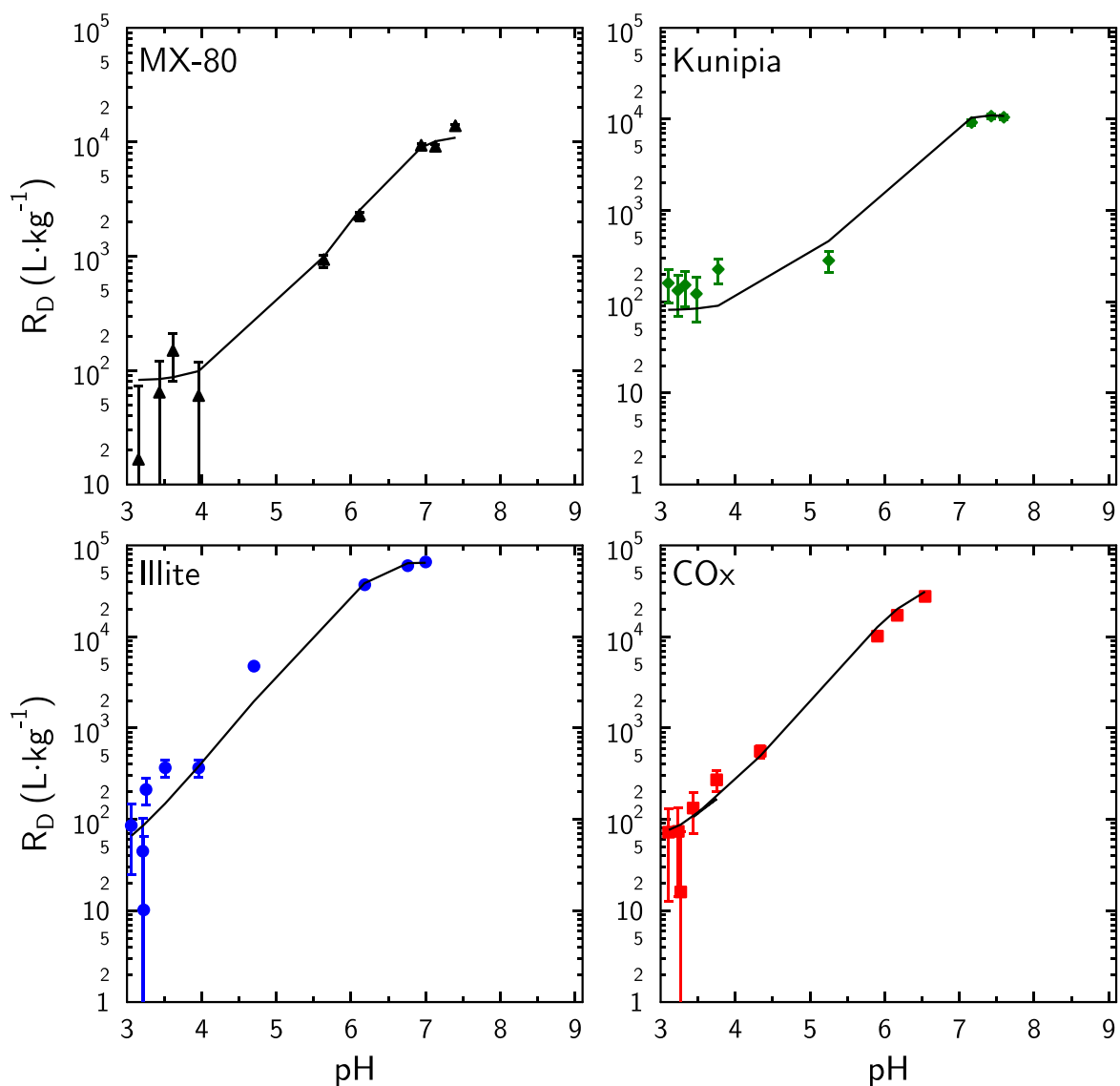


Figure 7. Model predicting Pb adsorption on the four clay samples at 67°C. Parameters are given in Table 2. Total Pb concentration: 1 μM . Solid/liquid ratio: 1 $\text{g}\cdot\text{L}^{-1}$. Background electrolyte: NaCl 0.1 M.

4.3. Comparison with literature data

The predictions of the model were tested with Pb adsorption literature data obtained with different montmorillonite, bentonite and illite samples in a range of experimental conditions (Table 3).

Table 3: Experimental conditions of Pb absorption experiments described in the literature

Clay Type	Clay material preparation procedure	pH	Background electrolyte (M)	$[\text{Pb}]_{\text{tot}}$ (μM)	R_{SL} ($\text{g}\cdot\text{L}^{-1}$)	Reference
SWy-2 Mont.	None	3–11	0.001–0.1 NaNO_3	0.1–50	0.5	(Akafia et al. 2011)
Fithian illite	< 2 μm NaNO_3 treated	3–8	0.001–0.1 NaNO_3	50	2.97	(Gu and Evans 2007)

MX-80 Mont	None	1-12	0.01	NaNO ₃	48.3	0.2; 0.4	(Xu et al. 2008)
Wyoming	< 2 µm	3- 9	0.001	0.1	48.8	1.5	(Gu et al. 2010)
Mont.	NaNO ₃ treated			NaNO ₃			
Chinese	< 2 µM	2-12	0.001-0.1		72.5	0.5	(Yang et al. 2010)
bentonite	1.0 M NaCl			NaClO ₄			
	treated						

502

503 The data from Akafia et al. (2011), which were obtained with Swy-2 montmorillonite, were
504 adequately predicted with this very simple model (Figure 8). As for the modeling of the data
505 obtained in this study, the presence of a constant DIC concentration of 0.25 mM in all pH
506 range (due to atmospheric CO₂ contamination) and the possible precipitation of
507 hydrocerussite were also considered. Akafia et al.'s data at the highest total Pb concentration
508 (50 µM) and pH value above 6.5 were in quantitative agreement with a precipitation process
509 (Figure 8). Their data at low pH and low ionic strength (0.001 M NaNO₃ background
510 electrolyte) were reproduced, considering the presence of a low Mg²⁺ concentration
511 competing with Pb²⁺ for cation exchange sites. The Mg²⁺ concentration was fixed at 0.1 mM in
512 agreement with data reported in the literature in similar experimental conditions (Baeyens and
513 Bradbury 1995, Gu et al. 2010, Marty et al. 2011), and the same cation exchange selectivity
514 coefficient was attributed to Mg²⁺ and to Pb²⁺ (Fletcher and Sposito 1989, Tournassat et al.
515 2009). The presence of Mg²⁺ in solution (and on the exchanger at low background electrolyte
516 concentration) was due to the partial dissolution of the clay layers (Marty et al. 2011). The
517 competitive presence of Mg²⁺ for cation exchange sites cannot be avoided, and it cannot be
518 neglected in the modeling for data at low ionic strength (typically below 0.01) and low pH.
519 Finally, the data in the pH range 4 to 7 were very well fitted if the surface complexation site
520 density was increased from 0.01 to 0.02 mol·kg⁻¹ (Figure 8). Surface complexation site
521 density is related to the edge specific surface area of montmorillonite layers and not to the N₂-
522 BET surface area that lumps together external basal surface area and edge surface area (Metz
523 et al. 2005, Tournassat et al. 2015). According to Atomic Force Microscopy, Derivative
524 Isotherm measurements and potentiometric titration data, MX-80, Kunipia-P and Swy-2
525 montmorillonite have edge specific surface area values of ~7 – 12 m²·g⁻¹, ~5 m²·g⁻¹ and ~14 –
526 25 m²·g⁻¹ respectively (Duc et al. 2005, Yokoyama et al. 2005, Le Forestier et al. 2010,
527 Tournassat et al. 2015, 2016). This difference in surface area values is commensurable with
528 the modeled difference in site density between MX-80/Kunipia-P and Swy-2 samples.
529 Consequently, the agreement between the model predictions and the published data from
530 Akafia et al. (2011) indicated that three different reference montmorillonite samples – MX-
531 80, Kunipia-P, and Swy-2 – had similar Pb adsorption properties, MX-80 and Kunipia-P
532 having a smaller site density than Swy-2 because of their smaller edge specific surface area.

533 With the same modeling approach, the Pb adsorption data that were measured by Gu and
534 Evans (2007) with Fithian illite were predicted correctly up to pH 6.5 in the presence of
535 0.001-0.1 M NaNO₃ and of a 50 µM Pb total concentration. Above this pH value, the model
536 overestimated the measured adsorption values, but this discrepancy may fall in the range of
537 data uncertainty: first, it was difficult to estimate the uncertainty in the measurement itself,
538 and second, data digitization may have introduced some bias especially for data at retention
539 values close to 100%, for which the discrepancy is the largest. A better data fit was obtained if
540 the site density was reduced from 0.035 to 0.025 mmol·kg⁻¹ (Figure 9). Because this
541 difference in site density is small, it can be concluded that Fithian illite and IdP had similar Pb
542 adsorption properties.

Some other literature data were not compatible with this model prediction. Xu et al. (2008) studied Pb adsorption on non-purified MX-80 bentonite, i.e. a material similar to the materials used in this study, except that it contained additional mineral impurities such as quartz, cristobalite, feldspar and calcite, which were partly removed during the sample preparation procedure in this study. Xu et al. (2008) used a high Pb to clay ratio (total Pb concentration was 48.3 μM and solid/liquid ratio was 0.2 or 0.4 $\text{g}\cdot\text{L}^{-1}$). In the experiment with 50 μM total Pb concentration and a clay concentration of 1 $\text{g}\cdot\text{L}^{-1}$ and $I=0.01\text{ M NaNO}_3$, a site ($>S$) saturation effect was observed at $\text{pH} < 6.5$ that made it possible to refine a site density value at $\sim 0.01\text{ mol}\cdot\text{kg}^{-1}$ (Figure 5). At pH values greater than 6.5, Pb precipitation occurred in these experimental conditions. In the experiments of Xu et al. (2008), such site saturation did not occur (Figure 10). If their data were modeled with a surface complexation model, the site density should have been as high as $0.15\text{ mol}\cdot\text{kg}^{-1}$. Because the edge specific surface area of MX-80 is $\sim 8\text{ m}^2\cdot\text{g}^{-1}$, this site density would correspond to a surface occupancy of more than 11 atoms per nm^2 . This value is unrealistic and indicates clearly that additional processes such as (co-)precipitation and/or surface precipitation must have occurred during their experiments. The same conclusion can be made for the data of Yang et al. (2010), who reported similar data for Pb retention on a Na-bentonite from Lin'an (from China) at different ionic strength (0.001-0.1) with different background electrolytes and initial Pb concentration of 72.5 μM . Why such processes occurred in their experiments and not in the experiments of this study or those of Akafia et al. (2011) remains unclear. Based on extended X-ray absorption fluorescence spectroscopy measurements (EXAFS), Strawn and Sparks (1999) suggested the presence of Pb-Pb dimer on montmorillonite because of surface multilayer adsorption and/or enhanced polymer formation due to nucleation from the clay. Surface precipitation of divalent metals on clay mineral surfaces has been repeatedly observed with spectroscopic techniques, especially with polarized EXAFS (P-EXAFS) (Scheidegger et al. 2001, Schlegel et al. 2001, D'Amico et al. 2002, Schlegel and Manceau 2006). Polynuclear Pb species also formed at pH's above 4.5 in the presence of high total Pb concentration sorbed on amorphous silica, a mineral impurity that is frequently present in montmorillonite samples (Elzinga and Sparks 2002). Therefore, the formation of polynuclear Pb species at the surfaces of clay minerals or of mineral impurities may explain the results from Yang et al. (2010), and Xu et al. (2008).

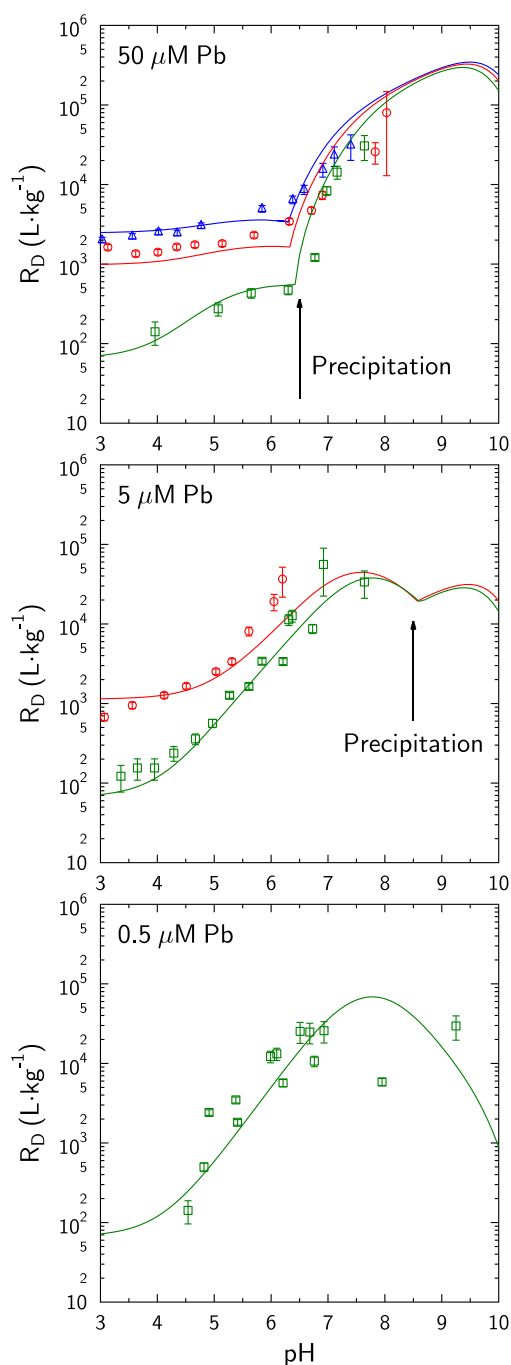
The data from Gu et al. (2010) onto Na-montmorillonite could only be fitted with an increase of the site density from 0.01 to $0.05\text{ mol}\cdot\text{kg}^{-1}$ (Figure S-4). It is unclear if this increase in site density may be justified or not: this site density corresponds to an edge specific surface area of $\sim 30\text{-}40\text{ m}^2\cdot\text{g}^{-1}$ according to the calculations explained above. Gu et al. (2010) used the $<2\text{ }\mu\text{m}$ fraction of an Upton (Wyoming, USA) montmorillonite, and applied an acid treatment at pH 3 for 5 h. This acid treatment could have formed new edge adsorption sites following the partial dissolution of the clay, and/or new mineral impurities such as amorphous silica. However, such a sample preparation effect was not apparent in the study carried out on Fithian illite by the same authors and with the same sample preparation procedure (Gu and Evans 2007).

According to crystallographic data, clay mineral edge surfaces can adsorb a maximum Pb monomer density of $d_{\text{mono}}=2\text{ atom}\cdot\text{nm}^{-2}$ (Tournassat et al. 2018). Above this threshold value,

the presence of Pb dimers, polymers, or (co-)precipitation at the surface or in solution is necessary to explain Pb retention values. SCM, for which only Pb monomer adsorption reactions are considered, should then be restricted to the interpretation of data that do not exceed this threshold value. The value of the edge specific surface area is however not well known for most of the investigated clay minerals. This value is also subject to variability because of the origin of the clay stock and/or on the clay preparation procedure. The specific surface area measured by BET cannot help to determine the specific surface area of edges. It is however possible to quantify a minimal edge specific surface area ($ESSA_{min}$ in $\text{m}^2\cdot\text{g}^{-1}$) that is necessary to explain the data according to:

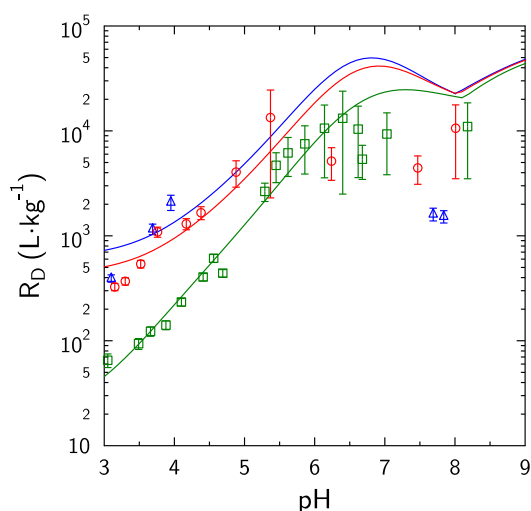
$$ESSA_{min} = \frac{C_{ads} \cdot N_A}{1000 \cdot d_{mono} \cdot 10^{18}} \quad (5)$$

where N_A is the Avogadro number ($6.022 \cdot 10^{23} \text{ mol}^{-1}$). If $ESSA_{min}$ exceeds the maximum reported value of edge specific surface area (i.e. $25 \text{ m}^2\cdot\text{g}^{-1}$ for montmorillonite), or the BET surface area value (which always exceeds the edge specific surface area) in the presence of conditions where only surface complexation is expected, i.e. high electrolyte background concentration to minimize cation exchange and $\text{pH} < 6.5$ to prevent hydrocerussite precipitation, then it can be concluded that the data are not representative of surface complexation processes.

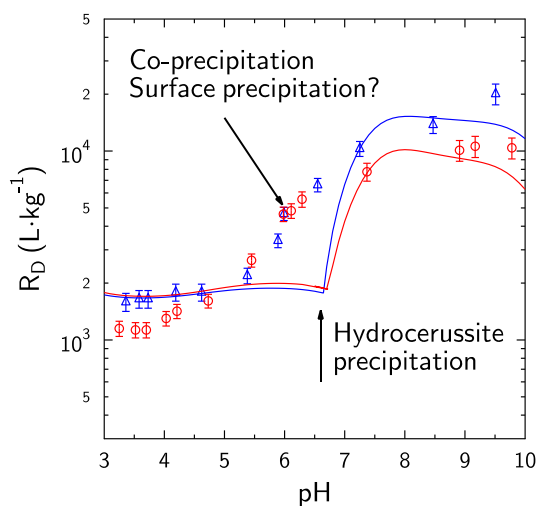


602

603 Figure 8. Prediction (lines) of the Pb adsorption data (symbols) on Swy-2 montmorillonite
 604 from Akafia et al. (2011), in the presence of a guessed DIC concentration of 0.25 mM, and of
 605 a guessed Mg concentration of 0.1 mM. Solid/ liquid ratio: 0.5 g·L⁻¹. From top to bottom, Pb
 606 total concentration of 50 μM, 5 μM and 0.5 μM. Blue triangles and line: 0.001 M NaNO₃
 607 background electrolyte. Red circles and lines: 0.02 M NaNO₃ background electrolyte. Green
 608 squares and lines: 0.1 M NaNO₃ background electrolyte. Error bands were calculated based
 609 on a digitization error of ±1% on the adsorbed Pb percentage (original data were reported as
 610 percentage of adsorption vs. pH). Data with error bands larger than their corresponding R_D
 611 value were discarded.



612
 613 Figure 9. Prediction (lines) of the Pb adsorption data (symbols) on Fithian illite from Gu and
 614 Evans (2007), in the presence of a guessed DIC concentration of 0.25 mM, and of a guessed
 615 Mg concentration of 0.1 mM. Solid/liquid ratio: 2.97 g·L⁻¹. Pb total concentration = 50 μM.
 616 The site density was reduced to 0.025 mol·kg⁻¹ instead of 0.035 mol·kg⁻¹. Blue triangles and
 617 line: 0.001 M NaNO₃ background electrolyte. Red circles and lines: 0.01 M NaNO₃
 618 background electrolyte. Green squares and lines: 0.1 M NaNO₃ background electrolyte. Error
 619 bands were calculated based on a digitization error of ±1% on the adsorbed Pb percentage
 620 (original data were reported as percentage of adsorption vs. pH). Data with error bands larger
 621 than their corresponding R_D value were discarded.



622
 623 Figure 10. Comparison of this model prediction with the data from Xu et al. (2008) on MX-80
 624 bentonite at I= 0.01 M NaNO₃. The initial DIC concentration was adjusted at 0.02 mM to fit
 625 the data at high pH. Total Pb concentration was 48.3 μM. Blue triangles and line: data
 626 obtained with a solid/liquid ratio of 0.2 g·L⁻¹. Red circles and line: data obtained with a
 627 solid/liquid ratio of 0.4 g·L⁻¹. Error bands were calculated based on a digitization error of ±1%
 628 on the adsorbed Pb percentage (original data were reported as percentage of adsorption vs.
 629 pH).

5. Conclusion

The determination of surface complexation model (SCM) parameters for direct or indirect use in performance assessment calculations must be based on a critical review of the data published in the literature. In this study, the experiments showed that many experimental artifacts lead to misinterpretations of the processes underlying the measured R_D values. For example, the order of reagent addition can influence the result. In addition, correct interpretation of the data can be impeded by side reactions such as precipitation in the presence of carbonated species in solution. Dissolved inorganic carbon concentrations are seldom reported in the literature. This study revealed that most of the Pb adsorption data measured at pH above 6.5 may indeed be representative of precipitating Pb carbonate minerals (see data from Akafia et al. (2011) on Figure 8). This problem can be circumvented by using low initial Pb concentration (typically below $5\ \mu\text{M}$) so that hydrocerussite is not saturated in the investigated pH range. Unfortunately, only a small set of published data were obtained with initial Pb concentration below $5\ \mu\text{M}$. Most of them had total Pb concentration greater than or equal to $50\ \mu\text{M}$. In these conditions, the possible presence of surface polymerization/(co-)precipitation processes were highlighted. Inadequate experimental procedures can be detrimental to quantitative interpretations with SCM and thus, many Pb retention data that are published in the literature should not be used to calibrate SCM parameters, because these data may not be representative of a true adsorption equilibrium, but rather of (co-)precipitation or surface precipitation in conditions that can be barely met in a waste storage environment (e.g. data from Xu et al. (2008) and some data of Akafia et al. (2011)). This conclusion could be certainly extended to other divalent metallic cations for which precipitation in the presence of carbonate in solution has not been considered. The determination of surface complexation model parameters for PA should rely on preliminary building of an adequate adsorption database, where adequate means that all experimental conditions are met to quantify surface complexation only.

Acknowledgement

This work was supported by the French Radioactive Waste Management Agency (Andra) as part of the Andra-BRGM scientific partnership (CTEC project). We gratefully acknowledge Prof. Tsutomu Sato from Hokkaido University for providing the Kunipia-P sample and PSI-LES laboratory for providing the IdP sample.

Appendix A.

Supplementary information to this article can be found online. Supplementary information contains Figures S-1 to S-4 and the experimental data in 26 tables.

References:

- Akafia, M. M., T. J. Reich, and C. M. Koretsky. 2011. Assessing Cd, Co, Cu, Ni, and Pb Sorption on montmorillonite using surface complexation models. *Applied Geochemistry* 26:S154 – S157.
- Altmann, S. 2008. Geo'chemical research: A key building block for nuclear waste disposal safety cases. *Journal of Contaminant Hydrology* 102:174–179.
- Altmann, S., C. Tournassat, F. Goutelard, J.-C. Parneix, T. Gimmi, and N. Maes. 2012. Diffusion-driven transport in clayrock formations. *Applied Geochemistry* 27:463–478.
- Armitage, P. J., D. R. Faulkner, and R. H. Worden. 2013. Caprock corrosion. *Nature Geoscience* 6:79–80.
- Baeyens, B., and M. H. Bradbury. 1995. A quantitative mechanistic description of Ni, Zn and Ca sorption on Na-montmorillonite. Part I: Physico-chemical characterisation and titration measurements. . Paul Scherrer Institut (PSI), Villigen.
- Baeyens, B., and M. H. Bradbury. 1997. A mechanistic description of Ni and Zn sorption on Na-montmorillonite. Part I: Titration and sorption measurements. *Journal of Contaminant Hydrology* 27:199–222.
- Barbier, F., G. Duc, and M. Petit-Ramel. 2000. Adsorption of lead and cadmium ions from aqueous solution to the montmorillonite/water interface. *Colloids and Surfaces A-Physicochemical and Engineering Aspects* 166:153–159.
- Beaucaire, C., E. Tertre, E. Ferrage, B. Grenut, S. Pronier, and B. Madé. 2012. A thermodynamic model for the prediction of pore water composition of clayey rock at 25 and 80 °C – Comparison with results from hydrothermal alteration experiments. *Chemical Geology* 334:62–76.
- Borisover, M., and J. A. Davis. 2015. Chapter 2 - Adsorption of inorganic and organic solutes by clay minerals. Pages 33–70 in C. Tournassat, C. I. Steefel, I. C. Bourg, and F. Bergaya, editors. *Natural and Engineered Clay Barriers*. . Elsevier.
- Bourg, I. C., G. Sposito, and A. C. M. Bourg. 2007. Modeling the acid-base surface chemistry of montmorillonite. *Journal of Colloid and Interface Science* 312:297–310.
- Bradbury, M. H., and B. Baeyens. 1997. A mechanistic description of Ni and Zn sorption on Na-montmorillonite. Part II: modeling. *Journal of Contaminant Hydrology* 27:223–248.
- Bradbury, M. H., and B. Baeyens. 2000. A generalised sorption model for the concentration dependent uptake of caesium by argillaceous rocksbae. *Journal of Contaminant Hydrology* 42:141–163.
- Bradbury, M. H., and B. Baeyens. 2002. Porewater Chemistry in Compacted Re-Saturated MX-80 Bentonite: Physico-Chemical Characterisation and Geochemical Modelling.
- Bradbury, M. H., and B. Baeyens. 2005a. Modelling the sorption of Mn(II), Co(II), Ni(II), Zn(II), Cd(II), Eu(III), Am(III), Sn(IV), Th(IV), Np(V) and U(VI) on montmorillonite: Linear free energy relationships and estimates of surface binding constants for some selected heavy metals and actinides. *Geochimica et Cosmochimica Acta* 69:875–892.

- Bradbury, M. H., and B. Baeyens. 2005b. Experimental and modelling investigations on Na-illite: Acid-base behaviour and the sorption of strontium, nickel, europium and uranyl. . Nagra, National Cooperative for the Disposal of Radioactive Waste.
- Busch, A., S. Alles, Y. Gensterblum, D. Prinz, D. N. Dewhurst, M. D. Raven, H. Stanjek, and B. M. Krooss. 2008. Carbon dioxide storage potential of shales. *International Journal of Greenhouse Gas Control* 2:297–308.
- Chang, F. R. C., and G. Sposito. 1996. The electrical double layer of a disk-shaped clay mineral particle: effect of electrolyte properties and surface charge density. *Journal of Colloid and Interface Science* 178:555–564.
- Chapman, N., and A. Hooper. 2012. The disposal of radioactive wastes underground. *Proceedings of the Geologists' Association* 123:46–63.
- Charlet, L., and C. Tournassat. 2005. Fe(II)-Na(I)-Ca(II) cation exchange on montmorillonite in chloride medium; evidence for preferential clay adsorption of chloride “metal ion pairs in seawater. *Aquatic Geochemistry* 11:115–137.
- Chen, Z., G. Montavon, Z. Guo, X. Wang, S. Razafindratsima, J.-C. Robinet, and C. Landesman. 2014a. Approaches to surface complexation modeling of Ni (II) on Callovo-Oxfordian clayrock. *Applied Clay Science* 101:369–380.
- Chen, Z., G. Montavon, S. Ribet, Z. Guo, J.-C. Robinet, K. David, C. Tournassat, B. Grambow, and C. Landesman. 2014b. Key factors to understand in-situ behavior of Cs in Callovo-Oxfordian clay-rock (France). *Chemical Geology* 387:47–58.
- Dähn, R., A. M. Scheidegger, A. Manceau, M. Schlegel, B. Baeyens, M. H. Bradbury, and M. schl. Morales. 2002. Neoformation of Ni phyllosilicate upon Ni uptake on montmorillonite: a kinetics study by powder and polarized extended X-ray absorption fine structure spectroscopy. *Geochimica et Cosmochimica Acta* 66:2335–2347.
- Davis, J. A., J. A. Coston, D. B. Kent, and C. C. Fuller. 1998. Application of the surface complexation concept to complex mineral assemblages. *Environmental Science and Technology* 32:2820–2828.
- Davis, J. A., and D. Kent. 1990. Surface complexation modeling in aqueous geochemistry. *Reviews in Mineralogy and Geochemistry* 23:177–260.
- Davis, J. A., D. E. Meece, M. Kohler, and G. P. Curtis. 2004. Approaches to surface complexation modeling of Uranium(VI) adsorption on aquifer sediments. *Geochimica et Cosmochimica Acta* 68:3621–3641.
- Druteikien, R., J. Šapolait, Ž. Ežerinskis, and L. Juodis. 2017. Batch-type study of Cs, Co, and Tc binding with hydrated cement under hyperalkaline conditions. *Journal of Radioanalytical and Nuclear Chemistry*:1–9.
- Duc, M., F. Gaboriaud, and F. Thomas. 2005. Sensitivity of the acid-base properties of clays to the methods of preparation and measurement: 1. Literature review. *Journal of Colloid and Interface Science* 289:139–147.
- Dzombak, D. A., and F. M. M. Morel. 1990. Surface complexation modeling-Hydrous ferric oxide. Page 393. . New York.
- Echeverría, J. C., I. Zarranz, J. Estella, and J. J. Garrido. 2005. Simultaneous effect of pH, temperature, ionic strength, and initial concentration on the retention of lead on illite. *Applied Clay Science* 30:103–115.
- Elzinga, E. J., and D. L. Sparks. 2002. X-ray absorption spectroscopy study of the effects of pH and ionic strength on Pb (II) sorption to amorphous silica. *Environmental science & technology* 36:4352–4357.
- Fletcher, P., and G. Sposito. 1989. The chemical modeling of clay/electrolyte interactions for montmorillonite. *Clay Minerals* 24:375–391.

- Le Forestier, L., F. Muller, F. Villiéras, and M. Pelletier. 2010. Textural and hydration properties of a synthetic montmorillonite compared with a natural Na-exchanged clay analogue. *Applied Clay Science* 48:18–25.
- Gaboreau, S., F. Claret, C. Crouzet, E. Giffaut, and C. Tournassat. 2012. Caesium uptake by Callovian–Oxfordian clayrock under alkaline perturbation. *Applied Geochemistry* 27:1194–1201.
- Gaboreau, S., J.-C. Robinet, and D. Prêt. 2016. Optimization of pore network characterization of compacted clay materials by TEM and FIB/SEM imaging. *Microporous and Mesoporous Materials* 224:116–128.
- Gailhanou, H., C. Lerouge, M. Debure, S. Gaboreau, E. C. Gaucher, S. Grangeon, J.-M. Grenèche, M. Kars, B. Madé, N. C. M. Marty, F. Warmont, and C. Tournassat. 2017. Effects of a thermal perturbation on mineralogy and pore water composition in a clay-rock: an experimental and modeling study. *Geochimica et Cosmochimica Acta* 197:193–214.
- Gailhanou, H., J. C. van Miltenburg, J. Rogez, J. Olives, M. Amouric, E. C. Gaucher, and P. Blanc. 2007. Thermodynamic properties of anhydrous smectite MX-80, illite IMt-2 and mixed-layer illite-smectite ISCz-1 as determined by calorimetric methods. Part I: Heat capacities, heat contents and entropies. *Geochimica et Cosmochimica Acta* 71:5463–5473.
- Gaucher, E., C. Robelin, J.-M. Matray, G. Negrel, Y. Gros, J. F. Heitz, A. Vinsot, H. Rebours, A. Cassabagnere, and A. Bouchet. 2004. ANDRA underground research laboratory: Interpretation of the mineralogical and geochemical data acquired in the Callovian-Oxfordian Formation by investigative drilling. *Physics and Chemistry of the Earth, Parts A/B/C* 29:55–77.
- Giffaut, E., M. Grivé, P. Blanc, P. Vieillard, E. Colàs, H. Gailhanou, S. Gaboreau, N. Marty, B. Madé, and L. Duro. 2014. Andra thermodynamic database for performance assessment: ThermoChimie. *Applied Geochemistry* 49:225–236.
- Goldberg, S. 2013. Surface complexation modeling. Reference Module in Earth Systems and Environmental Sciences, Elsevier.
- Grangeon, S., A. Vinsot, C. Tournassat, C. Lerouge, E. Giffaut, S. Heck, N. Groschopf, M. A. Denecke, S. Wechner, and T. Schäfer. 2015. The influence of natural trace element distribution on the mobility of radionuclides. The exemple of nickel in a clay-rock. *Applied Geochemistry* 52:155–173.
- Gu, X., and L. J. Evans. 2007. Modelling the adsorption of Cd(II), Cu(II), Ni(II), Pb(II), and Zn(II) onto Fithian illite. *Journal of Colloid and Interface Science* 307:317–325.
- Gu, X. Y., L. J. Evans, and S. J. Barabash. 2010. Modeling the adsorption of Cd (II), Cu (II), Ni (II), Pb (II) and Zn (II) onto montmorillonite. *Geochimica et Cosmochimica Acta* 74:5718–5728.
- Hiemstra, T., and W. H. Van Riemsdijk. 1996. A surface structural approach to ion adsorption: the charge distribution (CD) model. *Journal of Colloid and Interface Science* 179:488–508.
- Ikhsan, J., J. D. Wells, B. B. Johnson, and M. J. Angove. 2005. Surface complexation modeling of the sorption of Zn(II) by montmorillonite. *Colloids and Surfaces A-Physicochemical and Engineering Aspects* 252:33–41.
- Jackson, M. L. 1975. Soil chemical analysis - advanced course 2nd edition. . Published by the author, University of Wisconsin, Madison, Wisconsin.
- Kinniburgh, D., and D. Cooper. 2011. PhreePlot: Creating graphical output with PHREEQC.
- Marani, D., G. Macchi, and M. Pagano. 1995. Lead precipitation in the presence of sulphate and carbonate: Testing of thermodynamic predictions. *Water Research* 29:1085–1092.

- Marcussen, H., P. E. Holm, B. W. Strobel, and H. C. B. Hansen. 2009. Nickel sorption to goethite and montmorillonite in presence of citrate. *Environmental Science & Technology* 43:1122–1127.
- Marques Fernandes, M., A. Scheinost, and B. Baeyens. 2016. Sorption of trivalent lanthanides and actinides onto montmorillonite: Macroscopic, thermodynamic and structural evidence for ternary hydroxo and carbonato surface complexes on multiple sorption sites. *Water Research* 99:74–82.
- Marques Fernandes, M., N. Ver, and B. Baeyens. 2015. Predicting the uptake of Cs, Co, Ni, Eu, Th and U on argillaceous rocks using sorption models for illite. *Applied Geochemistry* 59:189–199.
- Marty, N. C. M., J. Cama, T. Sato, D. Chino, F. Villiéras, A. Razafitianamaharavo, J. Brendlé, E. Giffaut, J. M. Soler, E. C. Gaucher, and C. Tournassat. 2011. Dissolution kinetics of synthetic Na-smectite. An integrated experimental approach. *Geochimica et Cosmochimica Acta* 75:5849–5864.
- Metz, V., H. Raanan, H. Pieper, D. Bosbach, and J. Ganor. 2005. Towards the establishment of a reliable proxy for the reactive surface area of smectite. *Geochimica et Cosmochimica Acta* 69:2581–2591.
- Neuzil, C. E. 2013. Can shale safely host US nuclear waste? *Eos, Transactions American Geophysical Union* 94:261–262.
- Parkhurst, D. L., and C. A. J. Appelo. 2013. Description of Input and Examples for PHREEQC Version 3—a Computer Program for Speciation, Batch-reaction, One-dimensional Transport, and Inverse Geochemical Calculations.
- Richter, A., V. Brendler, C. Nebelung, T. E. Payne, and T. Brasser. 2009. Sorption Databases for Increasing Confidence in Performance Assessment. Pages 361–367 ASME 2009 12th International Conference on Environmental Remediation and Radioactive Waste Management. . American Society of Mechanical Engineers.
- Scheidegger, A., R. Dahn, A. Manceau, M. Schlegel, B. Baeyens, and M. H. Bradbury. 2001. Ni clay neoformation on montmorillonite surface. *Journal of Synchrotron Radiation* 8:533–535.
- Schlegel, M. L., and A. Manceau. 2006. Evidence for the nucleation and epitaxial growth of Zn phyllosilicate on montmorillonite. *Geochimica et Cosmochimica Acta* 70:901–917.
- Schlegel, M. L., A. Manceau, L. Charlet, D. L. Chateigner, and J. L. Hazemann. 2001. Sorption of metal ions on clay minerals. III. Nucleation and epitaxial growth of Zn phyllosilicate on the edges of hectorite. *Geochimica et Cosmochimica Acta* 65:4155–4470.
- Secor, R. B., and C. J. Radke. 1985. Spillover of the diffuse double layer on montmorillonite particles. *Journal of Colloid and Interface Science* 103:237–244.
- Sipos, P., T. Németh, V. K. Kis, and I. Mohai. 2008. Sorption of copper, zinc and lead on soil mineral phases. *Chemosphere* 73:461–469.
- Sposito, G. 1984. The surface chemistry of soils. Page 223. . Oxford University Press, New York.
- Stockmann, M., V. Brendler, J. Schikora, S. Britz, J. Flügge, and U. Noseck. 2012. Smart Kd-concept based on surface complexation modeling. *Mineral. Mag* 76:2412.
- Strawn, D. G., and D. L. Sparks. 1999. The use of XAFS to distinguish between inner-and outer-sphere lead adsorption complexes on montmorillonite. *Journal of Colloid and Interface Science* 216:257–269.
- Tachi, Y., and K. Yotsuji. 2014. Diffusion and sorption of Cs⁺, Na⁺, I⁻ and HTO in compacted sodium montmorillonite as a function of porewater salinity: Integrated sorption and diffusion model. *Geochimica et Cosmochimica Acta* 132:75–93.

- Tertre, E., C. Beaucaire, N. Coreau, and A. Juery. 2009. Modelling Zn(II) sorption onto clayey sediments using a multi-site ion-exchange model. *Applied Geochemistry* 24:1852–1861.
- Tertre, E., G. Berger, S. Castet, M. Loubet, and E. Giffaut. 2005. Experimental sorption of Ni^{2+} , Cs^+ and Ln^{3+} onto a montmorillonite up to 150°C. *Geochimica et Cosmochimica Acta* 69:4937–4948.
- Tournassat, C., M. Bizi, G. Braibant, and C. Crouzet. 2011. Influence of montmorillonite tactoid size on Na-Ca cation exchange reactions. *Journal of Colloid and Interface Science* 364:443–454.
- Tournassat, C., I. C. Bourg, C. I. Steefel, and F. Bergaya. 2015. Chapter 1 - Surface Properties of Clay Minerals. Pages 5–31 in C. Tournassat, C. I. Steefel, I. C. Bourg, and F. Bergaya, editors. *Natural and Engineered Clay Barriers*. Elsevier.
- Tournassat, C., J. A. Davis, C. Chiaberge, S. Grangeon, and I. C. Bourg. 2016. Modeling the acid–base properties of montmorillonite edge surfaces. *Environmental Science & Technology* 50:13436–13445.
- Tournassat, C., H. Gailhanou, C. Crouzet, G. Braibant, A. Gautier, and E. C. Gaucher. 2009. Cation exchange selectivity coefficient values on smectite and mixed-layer illite/smectite minerals. *Soil Science Society of America Journal* 73:928–942.
- Tournassat, C., H. Gailhanou, C. Crouzet, G. Braibant, A. Gautier, A. Lassin, P. Blanc, and E. C. Gaucher. 2007. Two cation exchange models for direct and inverse modelling of solution major cation composition in equilibrium with illite surfaces. *Geochimica et Cosmochimica Acta* 71:1098–1114.
- Tournassat, C., S. Grangeon, P. Leroy, and E. Giffaut. 2013. Modeling specific pH dependent sorption of divalent metals on montmorillonite surfaces. A review of pitfalls, recent achievements and current challenges. *American Journal of Science* 313:395–451.
- Tournassat, C., R. M. Tinnacher, S. Grangeon, and J. A. Davis. 2018. Modeling uranium (VI) adsorption onto montmorillonite under varying carbonate concentrations: A surface complexation model accounting for the spillover effect on surface potential. *Geochimica et Cosmochimica Acta*:291–308.
- Turner, D. R., R. T. Pabalan, and F. P. Bertetti. 1998. Neptunium(V) sorption on montmorillonite: an experimental and surface complexation modeling study. *Clays and Clay Minerals* 46:256–269.
- Xu, D., X. L. Tan, C. L. Chen, and X. K. Wang. 2008. Adsorption of Pb(II) from aqueous solution to MX-80 bentonite: Effect of pH, ionic strength, foreign ions and temperature. *Applied Clay Science* 41:37–46.
- Yang, S., D. Zhao, H. Zhang, S. Lu, and X. L. and Yu Chen. 2010. Impact of environmental conditions on the sorption behavior of Pb (II) in Na-bentonite suspensions. *Journal of hazardous materials* 183.
- Yokoyama, S., M. Kuroda, and T. Sato. 2005. Atomic force microscopy study of montmorillonite dissolution under highly alkaline conditions. *Clays and Clay Minerals* 53:147–154.
- Zachara, J. M., and S. C. Smith. 1994. Edge complexation reactions of cadmium on specimen and soil-derived smectite. *Soil Science Society of America Journal* 58:762–769.

Highlights:

- Retention of Pb^{2+} on clay mineral surfaces was modeled with a simple surface complexation model.
- Model calibration requires experimental data in well-defined and well-controlled conditions.
- All experimental conditions are met to quantify surface complexation only
- Experimental artifacts, especially the presence of carbonate in solution, cause misinterpretation of measured retention values.
- Fully controlled experimental conditions are necessary for calibrating models for performance assessment studies.

Table 1
[Click here to download Table: Table 1.docx](#)

Initial Pb concentration (μM)	R_{SL} ($\text{g}\cdot\text{L}^{-1}$)	NaCl concentration (M)	pH range	T ($^{\circ}\text{C}$)
1	1	0.1	3-9	20*
10	1	0.1	3-9	20*
50	1	0.1	3-9	20*
1	0.5	0.025	3-9	20*
1	1	0.1	3-7	67

* Room temperature

Table 2
Click here to download Table: Table 2.docx

	Montmorillonite	Illite
Cation exchange		
CEC (X ⁻ site density) in mol·kg ⁻¹	0.78 ⁽¹⁾	0.2 ⁽²⁾
Reactions	log K	
2 XNa + Pb ²⁺ = X ₂ Pb + 2 Na ⁺	0.6 (0.9)	0.7 (0.9)
2 XNa + Mg ²⁺ = X ₂ Mg + 2 Na ⁺	0.6	0.7
2 XNa + Ca ²⁺ = X ₂ Ca + 2 Na ⁺	0.5	0.5
Edge surface complexation		
Site density (>S) in mol·kg ⁻¹	0.01	0.035
Reactions	log K	
>SOH = >SO ⁻ + H ⁺	-8.1	-6.6
>SOH + Pb ²⁺ = >SOPb ⁺ + H ⁺	0 (0.2)	0.6 (0.9)
>SOH + Pb ²⁺ + H ₂ O = >SOPb(OH) + 2H ⁺	Not necessary	-7.2 (-6.7)
⁽¹⁾ (Bradbury and Baeyens 2002)		
⁽²⁾ (Bradbury and Baeyens 2000)		

Table 3
[Click here to download Table: Table 3.docx](#)

Clay Type	Clay material preparation procedure	pH	Background electrolyte (M)	[Pb] _{tot} (μM)	R _{SL} (g.L ⁻¹)	Reference
SWy-2 Mont.	None	3–11	0.001–0.1 NaNO ₃	0.1–50	0.5	(Akafia et al. 2011)
Fithian illite	< 2 μm NaNO ₃ treated	3-8	0.001-0.1 NaNO ₃	50	2.97	(Gu and Evans 2007)
MX-80 Mont	None	1-12	0.01 NaNO ₃	48.3	0.2; 0.4	(Xu et al. 2008)
Wyoming Mont.	< 2 μm NaNO ₃ treated	3- 9	0.001 0.1 NaNO ₃	48.8	1.5	(Gu et al. 2010)
Chinese bentonite	< 2 μM 1.0 M NaCl treated	2-12	0.001-0.1 NaClO ₄	72.5	0.5	(Yang et al. 2010)

List of Figure Captions

Figure 1. Comparisons of experimental datasets for Pb retention at room temperature on MX-80, Kunipia-P, IdP and COx clay as a function of pH, ionic strength (0.025 M NaCl = closed symbols; 0.1 M NaCl = open symbols), and total Pb initial concentrations (triangle symbols: 1 μM ; circle symbols: 10 μM ; square symbols: 50 μM) (Details of the datasets are given in supporting information file).

Figure 2. Comparison of Pb retention on MX-80 (triangles), Kunipia (diamonds), IdP (circles) and COx clay (squares) at room temperature as a function of pH, in the presence of 0.1 M NaCl background electrolyte and a total Pb concentration of 1 μM .

Figure 3. Pb retention on MX-80 (triangles), Kunipia (diamonds), IdP (circles) and COx clay (squares) at room temperature (open symbols) and 67°C (closed symbols) as a function of pH, in the presence of 0.1 M NaCl background electrolyte and a total Pb concentration of 1 μM (Details of the datasets are given in supporting information file).

Figure 4. Top figure: Pb solid phase predominance as a function of pH and pCO_2 in the absence of adsorption processes. Minerals allowed to precipitate: cerussite (PbCO_3), hydrocerussite ($\text{Pb}_3(\text{CO}_3)_2(\text{OH})_2$), cotunnite (PbCl_2), laurionite (PbClOH), paralaurionite (PbClOH) and $\text{Pb}(\text{OH})_2(\text{s})$: Total Pb concentration: 50 μM ($\log [\text{Pb}]_{\text{tot}} = -4.3$). Middle figure: Contour plot of calculated Pb concentration in solution (\log_{10} scale) as a function of pH and pCO_2 . The color change between two contour lines indicates a change of 0.25 \log_{10} scale units. Bottom figure: Contour plot of calculated DIC concentration as a function of pH and pCO_2 (\log_{10} scale). Symbols correspond to experimental measurements in the presence (triangles) or absence (circles) of clay and with sample preparation in contact with atmosphere (white symbols) or in the glove-box (black symbols). The background electrolyte concentration is 0.1 M NaCl for all figures.

Figure 5. Modeling of Pb adsorption and precipitation at room temperature according to the parameters given in Table 2 for MX-80 (left) and illite (right).

Figure 6. Model prediction for Pb adsorption / precipitation on Kunipia-P (left) and COx clay (right) at room temperature. Model parameters for Kunipia-P are the same as for MX-80. Pb adsorption on COx clay was modeled with an illite surface contribution of 50% and a smectite surface (montmorillonite) contribution of 50%.

Figure 7. Model predicting Pb adsorption on the four clay samples at 67°C. Parameters are given in Table 2. Total Pb concentration: 1 μM . Solid/liquid ratio: 1 $\text{g}\cdot\text{L}^{-1}$. Background electrolyte: NaCl 0.1 M.

Figure 8. Prediction (lines) of the Pb adsorption data (symbols) on Swy-2 montmorillonite from Akafia et al. (2011), in the presence of a guessed DIC concentration of 0.25 mM, and of a guessed Mg concentration of 0.1 mM. Solid/ liquid ratio: 0.5 $\text{g}\cdot\text{L}^{-1}$. From top to bottom, Pb total concentration of 50 μM , 5 μM and 0.5 μM . Blue triangles and line: 0.001 M NaNO_3 background electrolyte. Red circles and lines: 0.02 M NaNO_3 background electrolyte. Green squares and lines: 0.1 M NaNO_3 background electrolyte. Error bands were calculated based on a digitization error of $\pm 1\%$ on the adsorbed Pb percentage (original data were reported as percentage of adsorption vs. pH). Data with error bands larger than their corresponding R_D value were discarded.

Figure 9. Prediction (lines) of the Pb adsorption data (symbols) on Fithian illite from Gu and Evans (2007), in the presence of a guessed DIC concentration of 0.25 mM, and of a guessed

Mg concentration of 0.1 mM. Solid/liquid ratio: $2.97 \text{ g}\cdot\text{L}^{-1}$. Pb total concentration = $50 \text{ }\mu\text{M}$. The site density was reduced to $0.025 \text{ mol}\cdot\text{kg}^{-1}$ instead of $0.035 \text{ mol}\cdot\text{kg}^{-1}$. Blue triangles and line: 0.001 M NaNO_3 background electrolyte. Red circles and lines: 0.01 M NaNO_3 background electrolyte. Green squares and lines: 0.1 M NaNO_3 background electrolyte. Error bands were calculated based on a digitization error of $\pm 1\%$ on the adsorbed Pb percentage (original data were reported as percentage of adsorption vs. pH). Data with error bands larger than their corresponding R_D value were discarded.

Figure 10. Comparison of this model prediction with the data from Xu et al. (2008) on MX-80 bentonite at $I = 0.01 \text{ M NaNO}_3$. The initial DIC concentration was adjusted at 0.02 mM to fit the data at high pH. Total Pb concentration was $48.3 \text{ }\mu\text{M}$. Blue triangles and line: data obtained with a solid/liquid ratio of $0.2 \text{ g}\cdot\text{L}^{-1}$. Red circles and line: data obtained with a solid/liquid ratio of $0.4 \text{ g}\cdot\text{L}^{-1}$. Error bands were calculated based on a digitization error of $\pm 1\%$ on the adsorbed Pb percentage (original data were reported as percentage of adsorption vs. pH).

Figure 1
[Click here to download Figure: Figure 1.pdf](#)

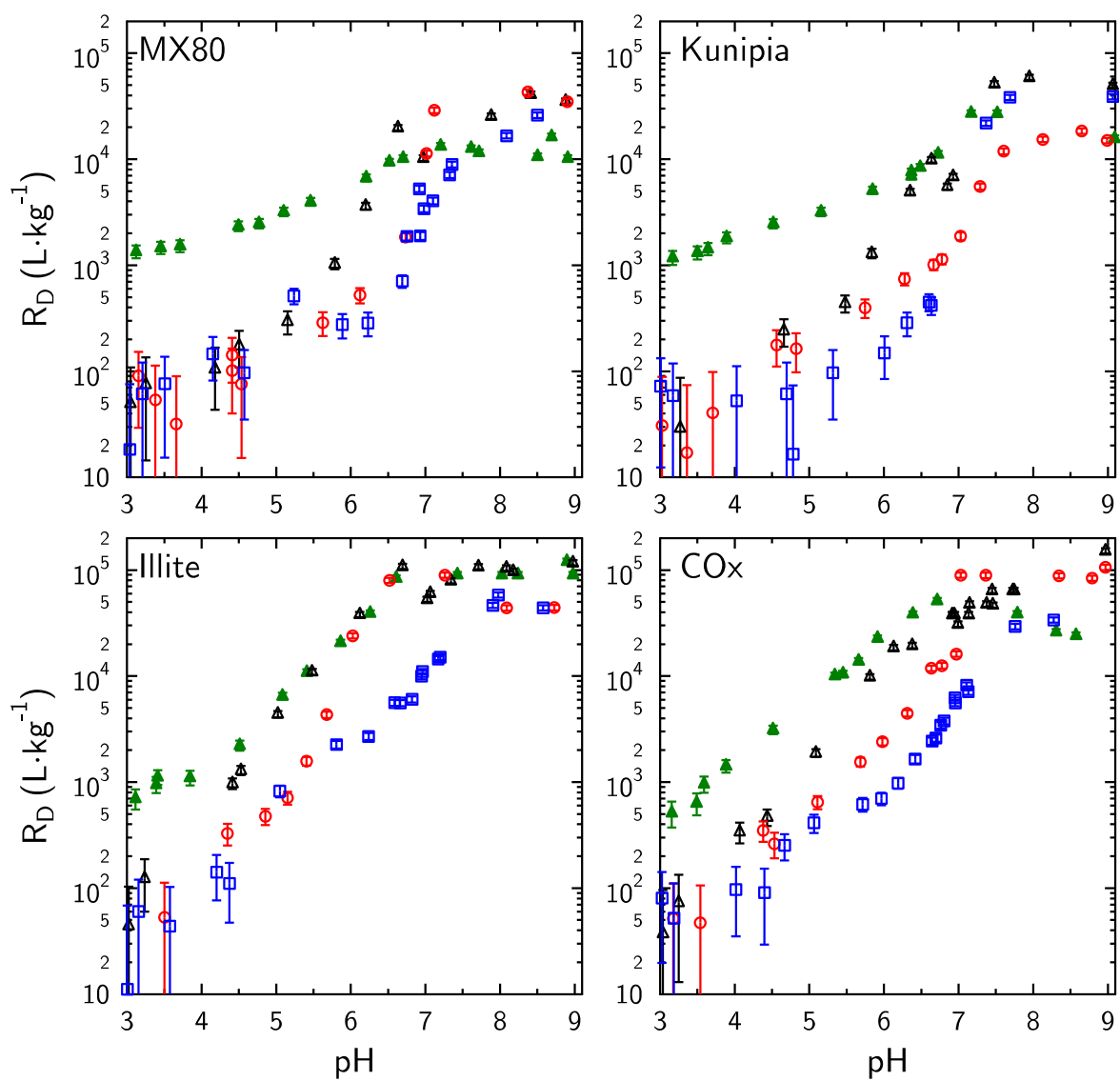


Figure 2
[Click here to download Figure: Figure 2.pdf](#)

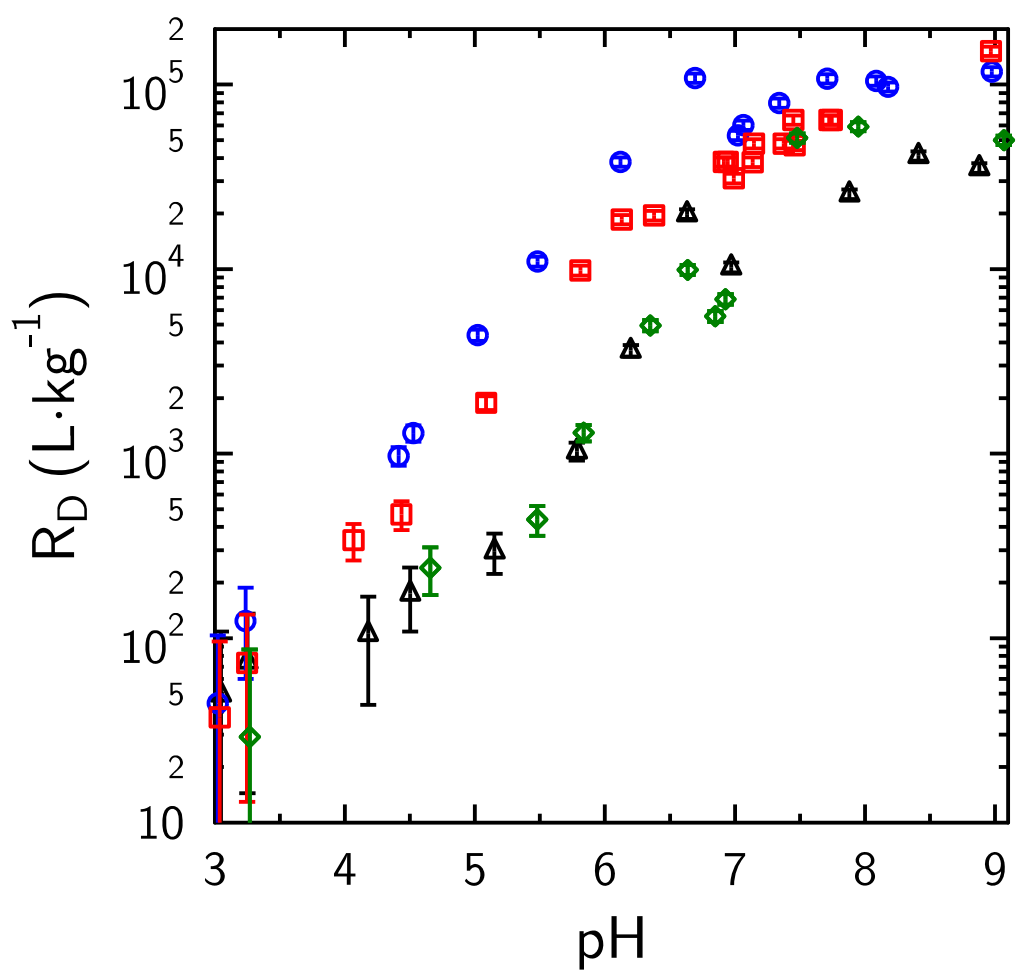


Figure 3
[Click here to download Figure: Figure 3.pdf](#)

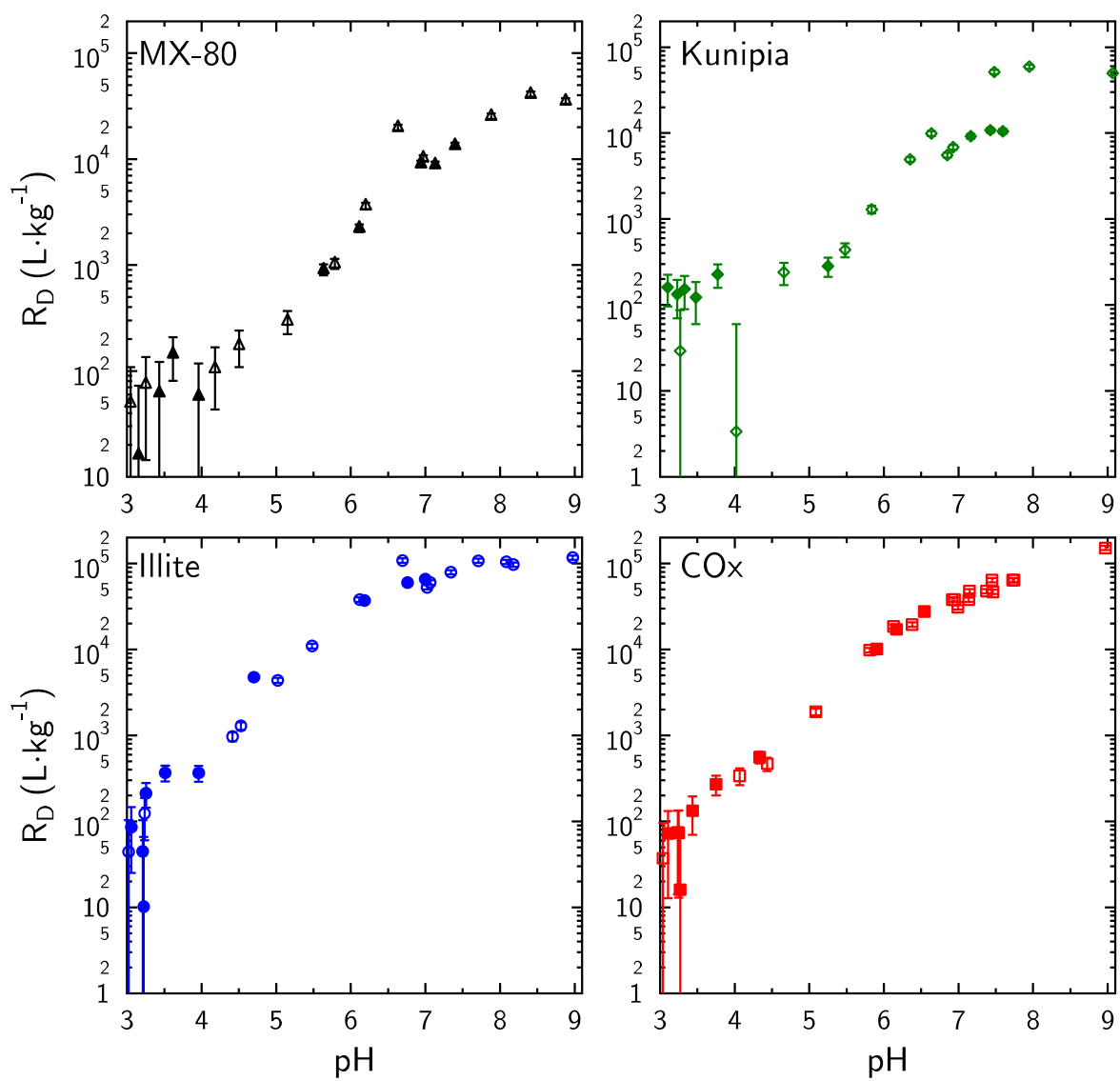


Figure 4

[Click here to download Figure: Figure 4.pdf](#)

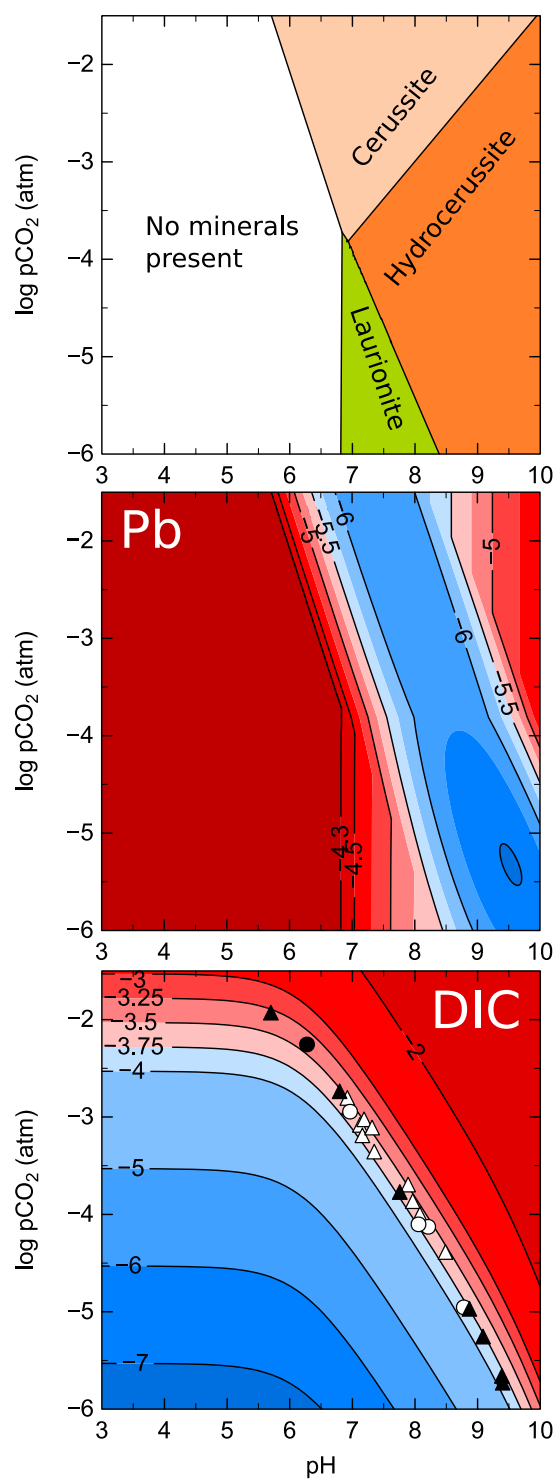
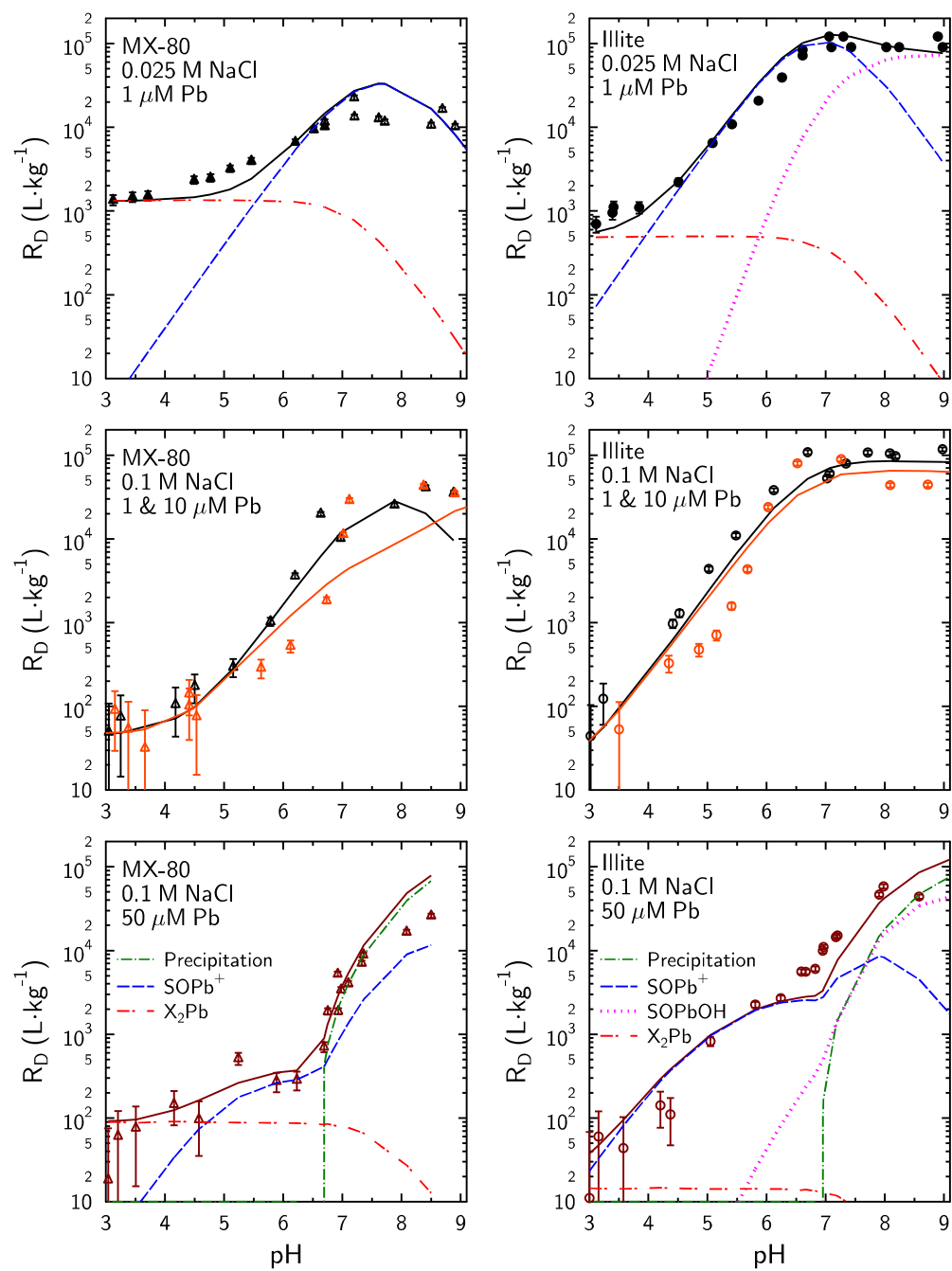
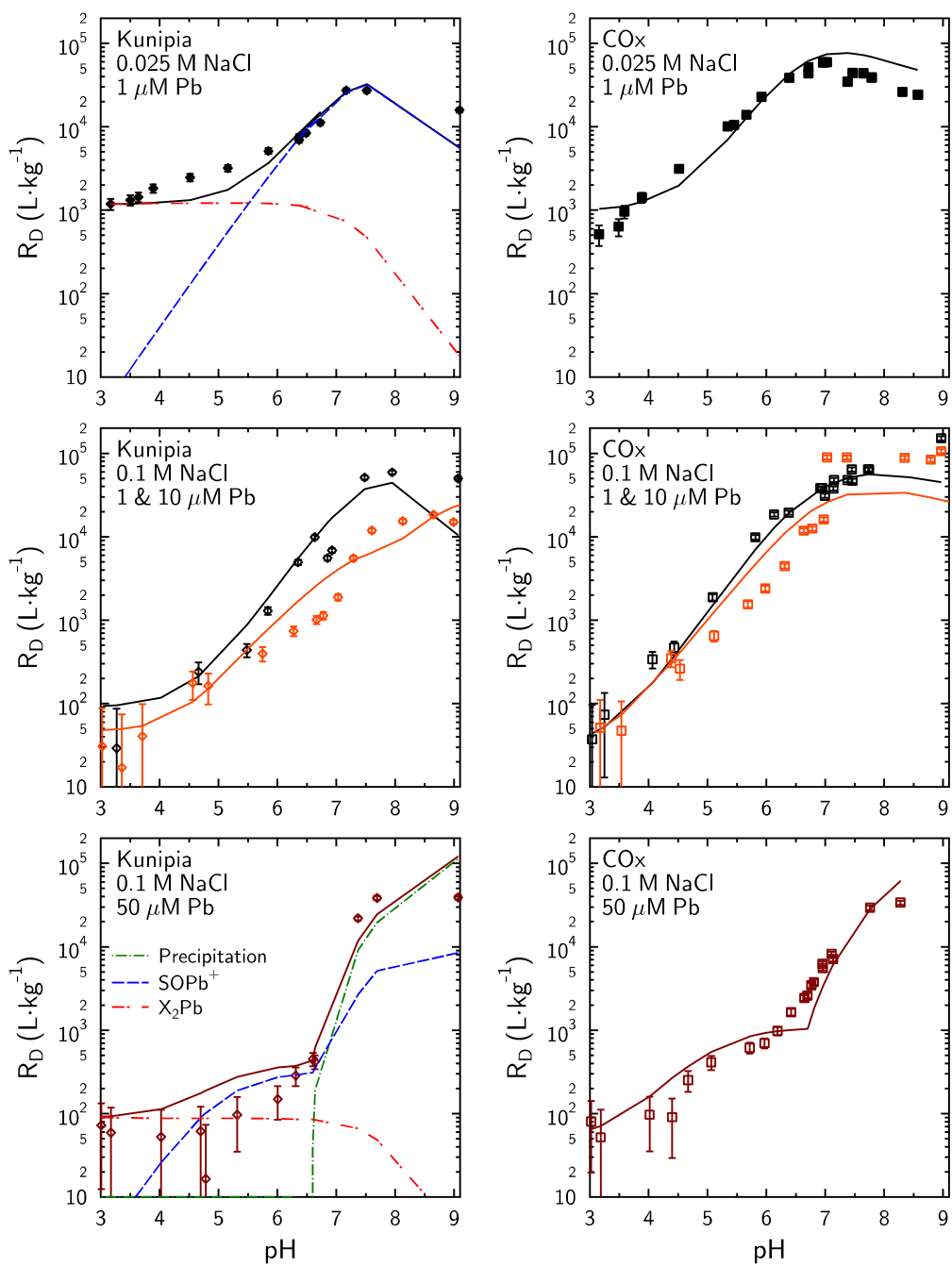


Figure 5
[Click here to download Figure: Figure 5.pdf](#)



Can you print Figure 5 in one page, if it is possible?

Figure 6
[Click here to download Figure: Figure 6.pdf](#)



Can you print Figure 6 in one page, if it is possible?

Figure 7

[Click here to download Figure: Figure 7.pdf](#)

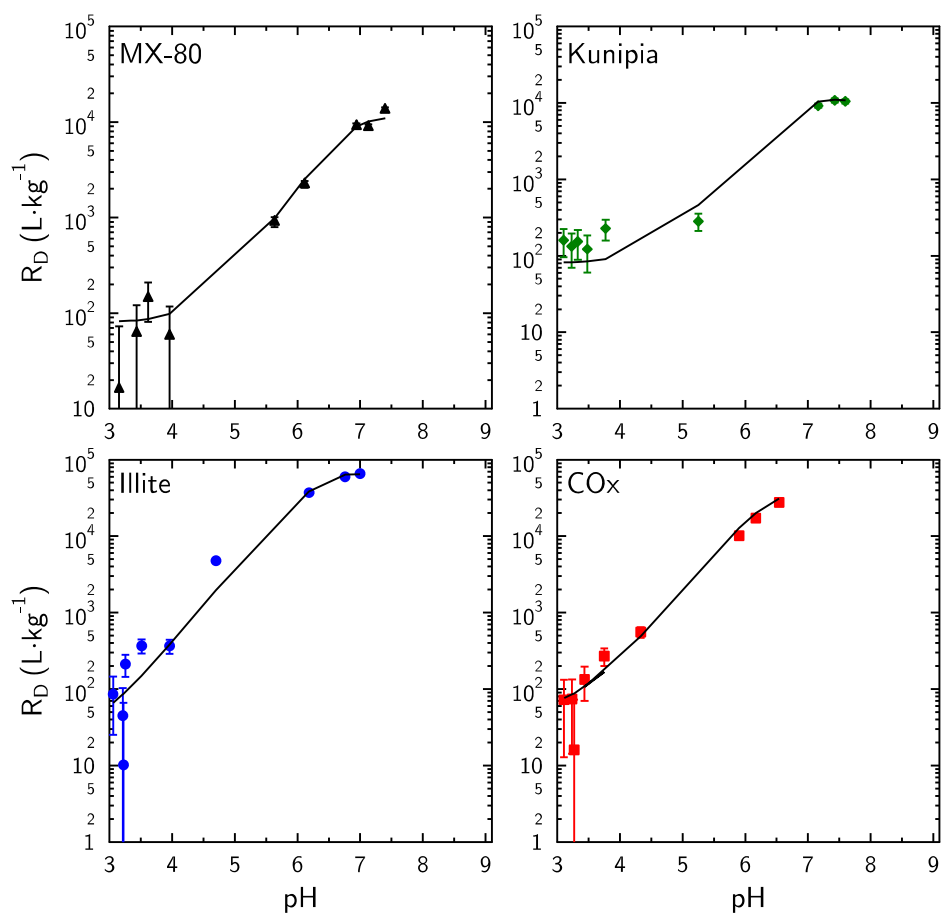


Figure 8
[Click here to download Figure: Figure 8.pdf](#)

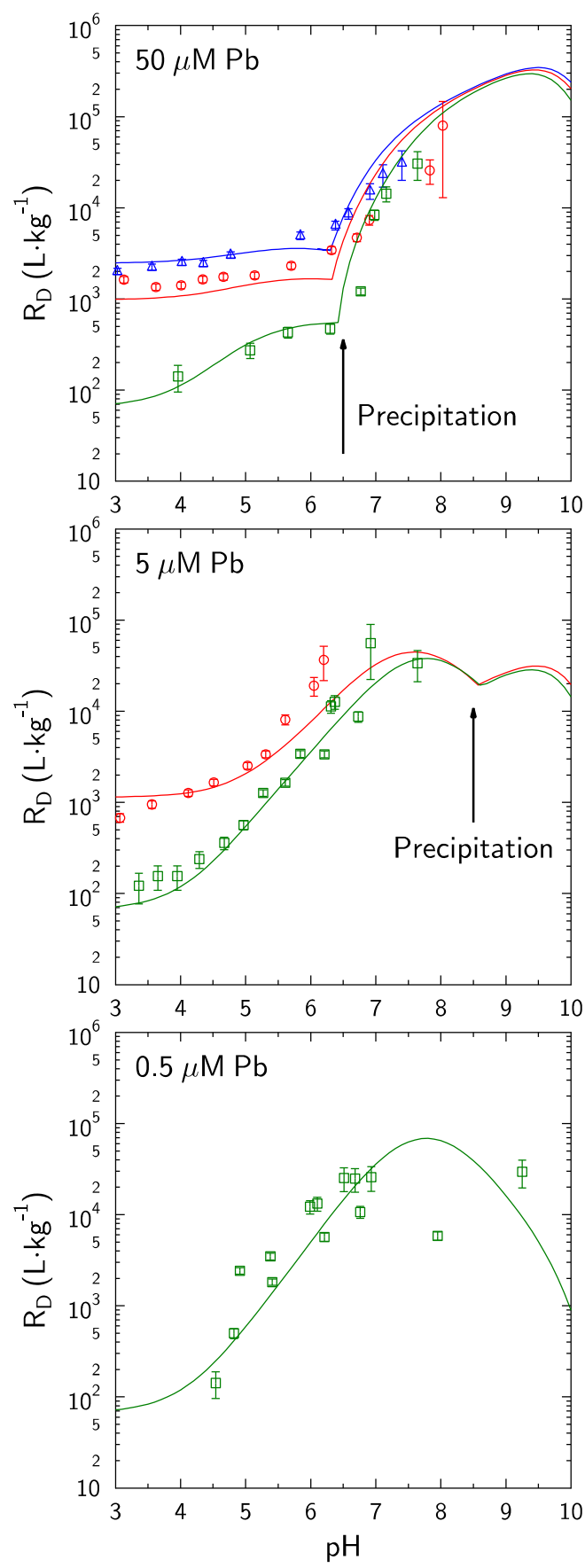


Figure 9

[Click here to download Figure: Figure 9.pdf](#)

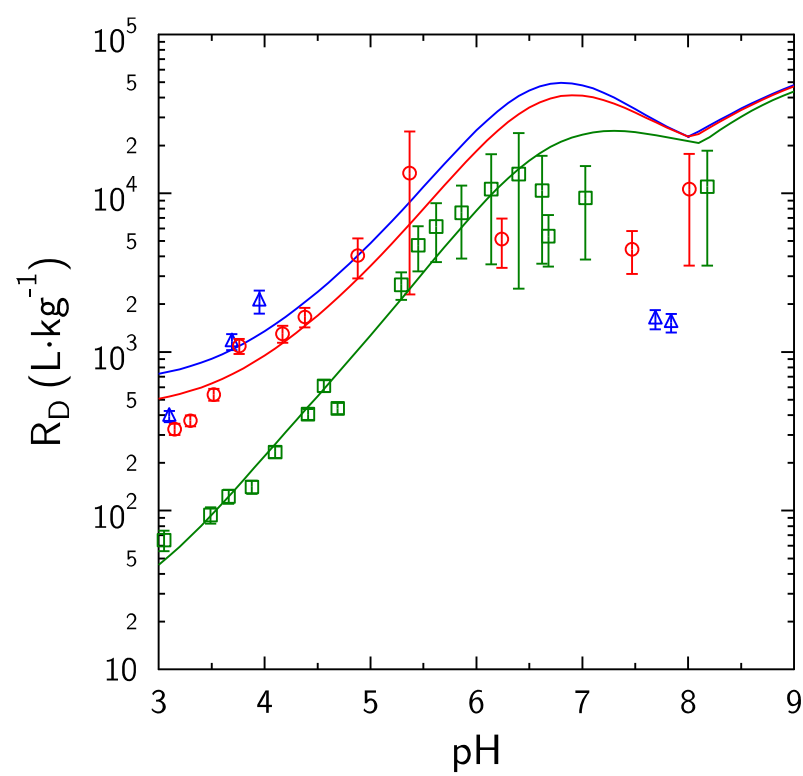
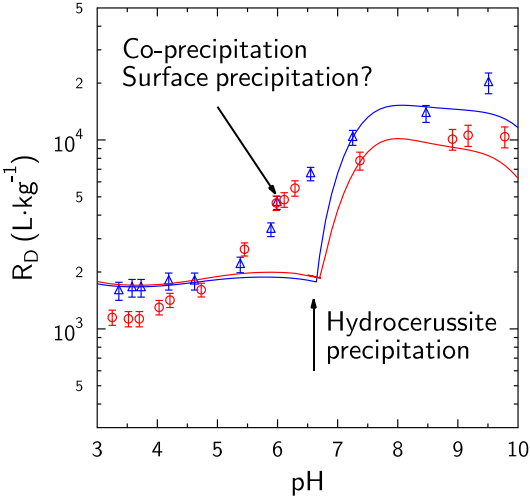


Figure 10

[Click here to download Figure: Figure 10.pdf](#)



Abstract

Surface complexation models (SCMs) have been developed in the last decades to describe metal ion sorption to clay minerals and especially to montmorillonite. In principle, these models can provide relevant information about sorption of radionuclides to be used in performance assessment (PA) of radioactive waste disposal systems. However, these SCMs have been developed in parallel with the acquisition of distinct adsorption datasets, which are not always consistent with each other. The objective of this study was to compare new experimental adsorption results with literature data to understand these discrepancies and to propose a SCM approach that could be amenable to determine sorption related retention parameters necessary for PA calculations. This study focused on lead (Pb) adsorption on montmorillonite, illite and in a natural clay (Callovo Oxfordian) as case studies of a strongly sorbing radionuclide that undergoes a range of retention processes depending on the chemical conditions. The experiments showed that many experimental artifacts lead to misinterpretations of the processes underlying the measured retention values. These include Pb precipitation in the presence of carbonate in solution. The determination of SCM parameters to provide sorption related information for PA of clay minerals should rely on preliminary building of an adequate adsorption database, where adequate means that all experimental conditions are met to quantify surface complexation only.

Background dataset for online publication only

[Click here to download Background dataset for online publication only: Supporting information-Revised2.pdf](#)